Journal of Advanced Research 51 (2023) 73–90

Contents lists available at ScienceDirect

Journal of Advanced Research

journal homepage: www.elsevier.com/locate/jare

Original Article

Maf1 is an intrinsic suppressor against spontaneous neural repair and functional recovery after ischemic stroke

Chi Kwan Tsang [a,b,1,*], Qiongjie Mi [a,c,1], Guangpu Su [a,c], Gum Hwa Lee [d,2], Xuemin Xie [a,c], Gabriella D'Arcangelo [d], Li'an Huang [a,c,e,*], X.F. Steven Zheng [b,*]

[a] Clinical Neuroscience Institute, The First Affiliated Hospital of Jinan University, Guangzhou 510630, China
[b] Rutgers Cancer Institute of New Jersey, 195 Little Albany Street, New Brunswick, NJ 08903, USA
[c] Department of Neurology, The First Clinical Medical School of Jinan University, Guangzhou, China
[d] Department of Cell Biology and Neuroscience, Rutgers, the State University of New Jersey, Piscataway, NJ 08854, USA
[e] Department of Neurology and Stroke Center, The First Affiliated Hospital, Jinan University Guangzhou, Guangdong, China

HIGHLIGHTS

- MAF1 is a novel intrinsic inhibitor of spontaneous recovery after ischemic stroke.
- MAF1 is upregulated and activated in neurons of peri-infarct cortex in the cerebral hemisphere.
- In addition to Pol III, MAF1 represses Pol II-transcribed CREB-related genes.
- MAF1 knockdown markedly enhances global protein synthetic capacity and CREB-mediated neural repair in peri-infarct cortex.
- Targeting MAF1 could potentiate neural plasticity and functional recovery after ischemic stroke and other CNS injuries.

GRAPHICAL ABSTRACT

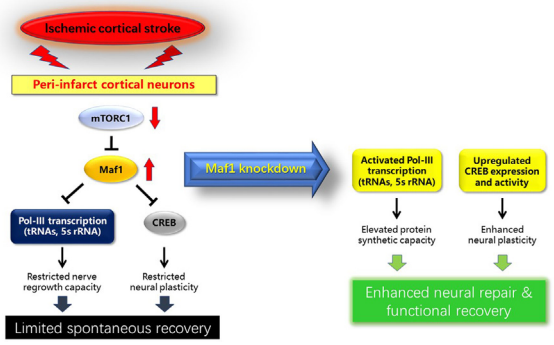

ARTICLE INFO

Article history:
Received 2 September 2022
Revised 28 October 2022
Accepted 13 November 2022
Available online 17 November 2022

Keywords:
Maf1
mTOR
Axon regeneration
Ischemic stroke
Functional recovery and neural repair

ABSTRACT

Introduction: Spontaneous recovery after CNS injury is often very limited and incomplete, leaving most stroke patients with permanent disability. Maf1 is known as a key growth suppressor in proliferating cells. However, its role in neuronal cells after stroke remains unclear.
Objective: We aimed to investigate the mechanistic role of Maf1 in spontaneous neural repair and evaluated the therapeutic effect of targeting Maf1 on stroke recovery.
Methods: We used mouse primary neurons to determine the signaling mechanism of Maf1, and the cleavage-under-targets-and-tagmentation-sequencing to map the whole-genome promoter binding sites of Maf1 in isolated mature cortical neurons. Photothrombotic stroke model was used to determine the therapeutic effect on neural repair and functional recovery by AAV-mediated Maf1 knockdown.
Results: We found that Maf1 mediates mTOR signaling to regulate RNA polymerase III (Pol III)-dependent rRNA and tRNA transcription in mouse cortical neurons. mTOR regulates neuronal Maf1 phosphorylation and subcellular localization. Maf1 knockdown significantly increases Pol III transcription, neurite outgrowth and dendritic spine formation in neurons. Conversely, Maf1 overexpression suppresses such activities. In response to photothrombotic stroke in mice, Maf1 expression is increased and accumulates

Peer review under responsibility of Cairo University.
* Corresponding authors at: Clinical Neuroscience Institute, First Affiliated Hospital of Jinan University, Guangzhou 510630, China (C.K.T.; L.H.).
E-mail addresses: tsangch@jnu.edu.cn (C.K. Tsang), tlian@jnu.edu.cn (L. Huang), zhengst@cinj.rutgers.edu (X.F. Steven Zheng).
[1] The authors equally contributed to this work.
[2] Present address: College of Pharmacy, Chosun University, Gwangju, South Korea.

https://doi.org/10.1016/j.jare.2022.11.007

in the nucleus of neurons in the peripheral region of infarcted cortex, which is the key region for neural remodeling and repair during spontaneous recovery. Intriguingly, Maf1 knockdown in the peri-infarct cortex significantly enhances neural plasticity and functional recovery. Mechanistically, Maf1 not only interacts with the promoters and represses Pol III-transcribed genes, but also those of CREB-associated genes that are critical for promoting plasticity during neurodevelopment and neural repair.
Conclusion: These findings indicate Maf1 as an intrinsic neural repair suppressor against regenerative capability of mature CNS neurons, and suggest that Maf1 is a potential therapeutic target for enhancing functional recovery after ischemic stroke and other CNS injuries.

Introduction

The morbidity rate of stroke has recently increased significantly. Among people over 60 years old, stroke is the major cause of permanent disability worldwide and results in substantial burden to medical care expenditures [1,2]. Although recent advances in intravenous thrombolysis and surgical thrombectomy have improved the treatment efficacy in the acute phase of ischemic stroke, only a small percentage of patients could benefit from these interventions because of their narrow therapeutic time windows [3]. Even for those patients who are eligible for receiving thrombolysis or intravascular thrombectomy, they may still suffer from serious sequelae with various degrees of disability [4]. Therefore, rehabilitation therapy after stroke is crucial for stroke patients. However, physical therapy can only partially restore the lost neurological functions, and there is no clinically approved drug therapy for boosting stroke recovery. Therefore, it is urgently needed to identify novel therapeutic targets and strategies for promoting nerve repair after stroke.

The brain exhibits amazing plasticity and self-healing potential after injury. After ischemic stroke, spontaneous recovery is triggered through molecular and cellular events such as transcriptional reprogramming that stimulates regeneration of axons and dendrite branching, synaptogenesis and circuit reconnection [4]. Preclinical studies have demonstrated that during the sub-acute phase of stroke, these spontaneous responses occur mainly in the peripheral region of infarcted tissue (peri-infarct region) [5]. Thus, the peri-infarct region is regarded as the viable therapeutic target for functional recovery. However, spontaneous recovery is often very limited and restricted, causing most stroke patients to suffer from permanent disability and deficit of neurological functions. A detailed understanding of the spontaneous recovery mechanisms is key to effective therapeutic approach aiming to enhance these spontaneous responses after stroke.

It is well recognized that CNS regeneration of axons after injury is constrained due to the suppressed capability of intrinsic growth in mature CNS neurons as well as the presence of extrinsic growth inhibitory factors such as Nogo and myelin-associated inhibitors secreted from astrocyte scars, myelin and fibrotic tissues [6]. However, merely blocking of these extrinsic inhibitory factors are not sufficient to trigger robust regeneration of axons after severe CNS injuries [6,7]. Compared with extrinsic factors, the intrinsic suppressive factors and mechanisms that restrict the neural regrowth and repair capacity after ischemic stroke remain relatively obscure. Emerging evidence from different models of CNS injury has demonstrated the vital role of neuronal intrinsic factors in promoting axon regeneration and neural repair. In particular, upregulation of mTOR signaling has been demonstrated to activate intrinsic mechanism of axon regeneration and neural repair in CNS injuries related to stroke and mechanical damages [6,8]. However, the underlying mechanism by the downstream effector of mTOR signaling for mediating neural repair has not been completely understood.

We previously discovered that Maf1 is the downstream substrate of TOR responsible for inhibition of transcription by RNA polymerase III (Pol III) in budding yeast [9]. We further found that TOR directly phosphorylates Maf1 in the cytoplasm under normal growth conditions, whereas Maf1 is dephosphorylated and translocated to the nucleus for repression of Pol III-dependent transcription under nutrient starvation conditions [9]. Subsequent studies by others in *Drosophila* and human cells have demonstrated that Maf1 regulation by TOR is highly conserved [10,11]. Maf1 is a major repressor of Pol III-dependent transcription that inhibits cell growth under various stress conditions [12–14]. In budding yeast, Maf1 deletion completely abolishes the nutrient deficiency-induced Pol III-transcriptional repression [15,16]. The inhibitory role of Maf1 in Pol III-transcription is also highly conserved in nematodes, fruit flies, rodents and humans [17,18]. In nematodes, knockdown of Maf1 increases tRNA levels, whereas overexpression of Maf1 decreases tRNA abundance and reduces the oogenesis and reproductive output [19]. In *Drosophila* larvae, knockdown of Maf1 increases overall protein synthesis, growth rate and body size [11]. In cancer cells, we and others showed that Maf1 expression is inversely correlated with proliferating rate, and that overexpression of Maf1 attenuates cellular growth [20,21]. Therefore, Maf1 is a key transcription regulator that inhibits the growth of proliferating cells.

In the process of neural repair after CNS injury, protein synthetic capacity in neurons is a determining factor for driving neurite regeneration [22–24]. Consistently, ribosome biosynthesis is essential for the growth and maintenance of dendrites [25]. It has been reported that mTOR signaling activity in adult retinal ganglion cells is downregulated after optic nerve injury, while knockdown of TSC1 or PTEN, the two upstream regulators of mTOR, reactivates mTOR signaling and promotes robust axon regeneration. Interestingly, Maf1 is highly expressed in neurons of cerebral cortex, hippocampus and retina [26,27], but its precise role in the nervous system has not been well-characterized. In the present study, we tested the hypothesis that Maf1 is an intrinsic regrowth inhibitor of neurons after ischemic stroke, and that ablation of Maf1 enhances neural plasticity and functional recovery. We first explored the functional roles of Maf1 in neurons. Then we examined the pathophysiological role of Maf1 in nerve repair and recovery. Finally, we evaluated the effect of Maf1 knockdown on functional recovery using the mouse ischemic stroke model.

Materials and Methods

Ethics statement

All animal experiments in this study were performed following the ethical policies and procedures approved by the ethics committee of the Animal Experimentation of Jinan University, China (Approval number: 2019285), and the Institutional Animal Care

and Use Committee (IACUC) at Rutgers University-Robert Wood Johnson Medical School, USA (Approval number: I11-049-7).

Animals

All mouse experimental procedures were complied with the guidelines recommended by the Animal Research: Reporting of In Vivo Experiments (ARRIVE). These animal experiments were also conducted in accordance with the recommendations suggested by the Guide for the Care and Use of Laboratory Animals of National Research Council. Approval was obtained by Rutgers University-Robert Wood Johnson Medical School-IACUC, and the Committee for Animal Experimentation of Jinan University. CD-1 timed pregnancy mice (Charles river, New Jersey, USA) were used for isolation of primary neurons. Adult male C57BL/6 mice used for the focal stroke models and female pregnancy mice used for isolation of primary neurons were obtained from the Laboratory Animal Science of Chinese Academy of Medical Science Institute (Guangzhou, China). All animals were housed in constant humidity and temperature in daily cycle of 12 h light and 12 h dark. Experimental animals were freely access to water and food *ad libitum* in their cages. In all experimental procedures including stroke surgeries, treatments and group allocation, mice were randomized and specific identity numbers were assigned by computer-generated random numbers for blinding the investigators who performed experimental procedures and analysis of data.

Mouse cortical ischemic stroke model

Photochemical thrombosis method was used for inducing the focal brain cortical ischemic stroke in adult male mice [28,29]. After anesthesia via inhalation of isoflurane, stereotaxic device was used for keeping the mice stable for coordination. Mouse skull was then exposed and a diode-pumped solid-state laser light with a wavelength of 532 nm, power of 0.5 mW, and diameter of 2-mm (GL532TA-100FC, Laser & Optics Century, Shanghai) was positioned at the left side 2.2 mm from fontanelle of the brain and 0.5 mm anteriorly. Rose Bengal (10 mg/mL) was administered intraperitoneally to 0.3 mL/30 g. After 5 min, the laser power of 80 mW was used for irradiation at the brain for 15 min. A Laser Speckle Contrast Imaging System (PeriCam PSI System, Perimed AB, Stockholm, Sweden) was used to monitor the blood flow in the brain to confirm the success of blood flow occlusion by the PT surgery. Rectal temperature of the mice was maintained at 37 °C during the surgery. Moues head skin was sutured after surgery and they were then transferred back to their cages for recovery.

Neuronal cell line, primary neuronal culture, treatments and transfection

Neuro2A cells were cultured in DMEM (high glucose, Thermo Fisher Scientific) supplemented with horse serum (10 %) (Thermo Fisher Scientific) and fetal bovine serum (5 %) (Thermo Fisher Scientific) in a 37 °C incubator supplied with 5 % CO_2. Differentiation of Neuro2A cells was induced by reducing the FBS concentration to 1 % in the same culture medium and incubation for 12 h. Papain Dissociation Kit (BioWorthington) was used for isolation and purification of primary cortical and hippocampal neurons from cerebral cortices and hippocampus dissected from the mouse embryos at embryonic stage of 15.5 day. The dissociated primary neurons were cultured as previously described [30]. Treatments of neurons with the indicated pharmacological inhibitors and/or Reelin or Mock conditioned medium were followed as described [31]. Transfection of primary neurons was performed using the Nucleofector with Amaxa Mouse Neuron Nucleofector Kit (Lonza).

Reagents, constructs and antibodies

Reagents involved in cell cultures were purchased from Thermo Fisher Scientific. Pharmacological inhibitors including rapamycin, rapalogs and other chemical inhibitors were purchased from LC Laboratories. Stable cell line CER was used to obtain the recombinant reelin in the conditioned medium as described [32], and the corresponding mock medium was obtained from the parental 293 EBNA cell line as described [31]. Maf1 specific 29mer shRNA constructs were expressed from retroviral GFP vector (pGFP-V-RS) (OriGene). Maf1 shRNA and scramble shRNA were expressed from AAV-PHP.eB vectors (PackGene Biotech). Vector overexpressing Myc-tagged Maf1 was constructed from pCMV6-AN-His-Myc vector (OriGene). Raptor shRNA was expressed from pLKO.1 vector (AddGene). Antibodies and other experimental reagents used in this study can be found in Table S3.

Isolation of total RNA, RT-PCR and real time PCR

RNA was extracted and purified as described previously [33]. RETROscript Kit (Ambion) was used for reverse transcription (RT) using random decamers according to the user instruction. TRIzol reagent was used for extraction of RNA from brain tissues and Evo M-MLV RT Mix kit (AG 11728) and SYBR Green Pro Taq HS qPCR kit (AG11701) were used for RT step and quantitative real time PCR, respectively. PCR was then used to amplify cDNA as described in the user menu. For real time PCR, the Rotor-Gene Q2 plex System (Qiagen) was used for the quantification of cDNA. To determine whether DNA contamination was present in the samples, the reverse transcriptase was omitted in parallel samples during cDNA synthesis as a control. For each sample, at least three technical replicates were used for setting up the reactions with the Rotor-Gene SYBR Green PCR Kit or SYBR Green Pro Taq HS qPCR kit (AG11701). The program consisted of one hold at 95 °C for 5 min, followed by 40 cycles of 5 s at 95 °C and 10 s at 60 °C was used for the thermocycling reactions. The melting curves were analyzed to ensure PCR products were specific, free from contamination and primer dimmers. We have tested several real-time PCR-specific primers for 5S pre-rRNA and found that they were not appropriate based on the melting curve analysis. Thus, we used conventional RT-PCR for quantification of 5S pre-rRNA expressions as described [34,35], whereas real time PCR was used for the expression analysis of all other genes. Levels of messenger RNA of the house keeping genes *GAPDH* or *ACT1* were used for the normalization purpose. Relative RNA levels were determined by standard curves method as described [36]. Primer sequences used for PCR in this study could be found in Table S4. The primer pairs used for measuring 5S rRNA and tRNA transcription detect their nascent transcripts which are processed rapidly during transcription and therefore can accurately reflect their transcription activity [34,35].

Western blot analysis

For tissue samples of mouse brain and neuronal cells, we used the RIPA buffer (Tris-HCL: 50 mM, pH 7.2, NaCl: 150 mM, NP-40: 1 %, EDTA: 2 mM, SDS: 0.1 %, PMSF: 0.1 mM, cocktails of protease and phosphatase inhibitor (Roche)) for lysis and protein extraction. Protein samples (5–30 μg/lane) were loaded onto SDS-PAGE (8–12 % according to protein size) and then transferred to PVDF membrane (Bio-Rad). TBST supplemented with 5 % milk was used to block the membranes for one hour. The blocked membrane was then incubated with specific primary antibodies in the same blocking buffer at 4 °C for 1 h to overnight, depending on the recommendation of antibody vendors. Primary antibodies used in this study included rabbit polyclonal anti-Maf1 antibody (NOVUS, #31617, 1:1,000), rabbit monoclonal anti-PSD9 (Cell Signaling Technology

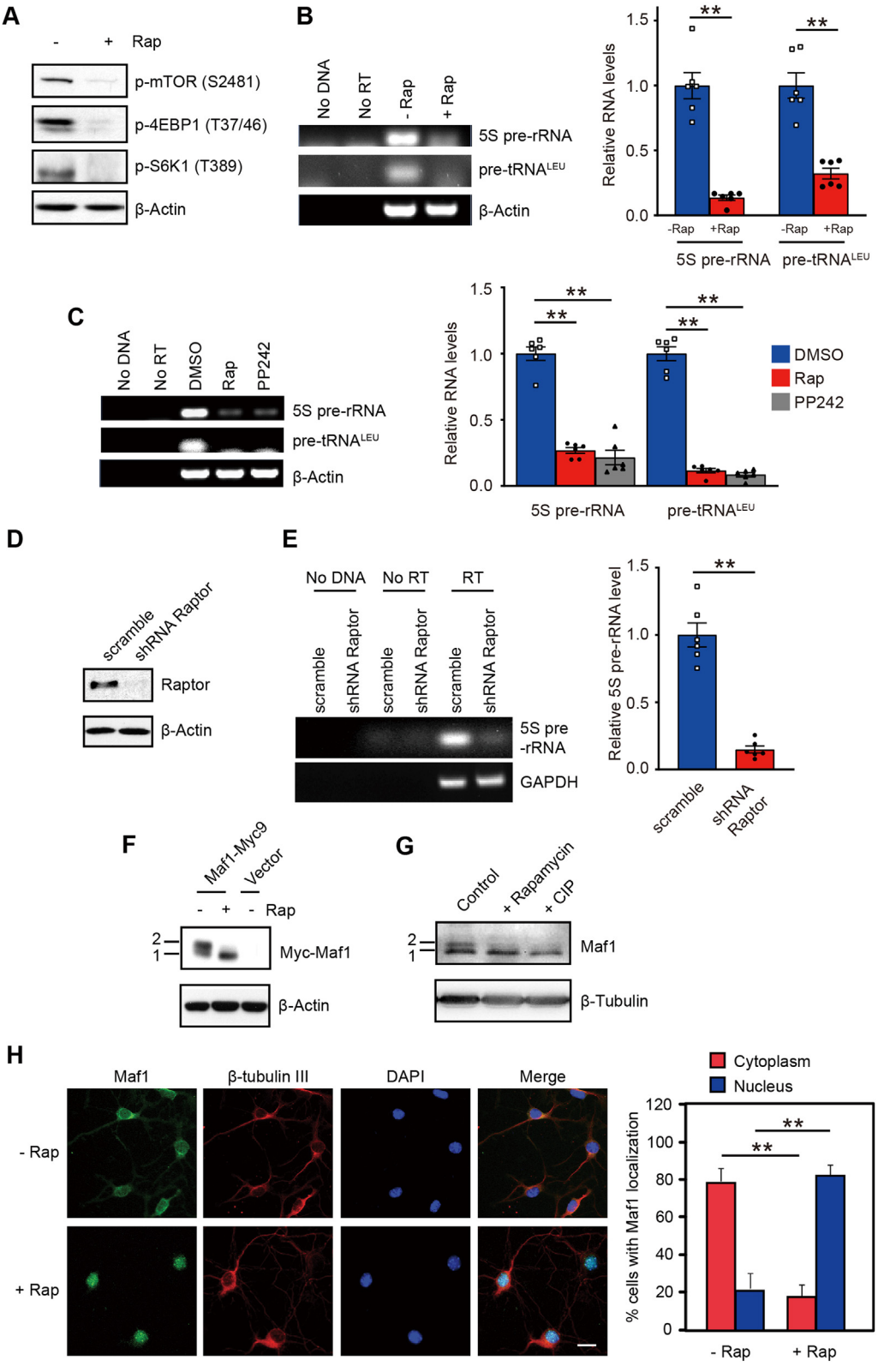
A
- + Rap
p-mTOR (S2481)
p-4EBP1 (T37/46)
p-S6K1 (T389)
β-Actin
B
No DNA
No RT
- Rap
+ Rap
5S pre-rRNA
pre-tRNALEU
β-Actin
Relative RNA levels
-Rap +Rap -Rap +Rap
5S pre-rRNA pre-tRNALEU
C
No DNA
No RT
DMSO
Rap
PP242
5S pre-rRNA
pre-tRNALEU
β-Actin
Relative RNA levels
DMSO
Rap
PP242
5S pre-rRNA pre-tRNALEU
D
scramble
shRNA Raptor
Raptor
β-Actin
E
No DNA No RT RT
scramble shRNA Raptor scramble shRNA Raptor scramble shRNA Raptor
5S pre -rRNA
GAPDH
Relative 5S pre-rRNA level
scramble shRNA Raptor
F
Maf1-Myc9 Vector
- + - Rap
Myc-Maf1
β-Actin
G
Control + Rapamycin + CIP
Maf1
β-Tubulin
H
Maf1 β-tubulin III DAPI Merge
- Rap
+ Rap
Cytoplasm
Nucleus
% cells with Maf1 localization
- Rap + Rap

(CST), #3450, 1:1,000), rabbit monoclonal anti-Synaptophysin (CST #36406, 1:1000), rabbit monoclonal anti-GAP43 (Signalway, #49013, 1:2,000), mouse monoclonal anti-NF160 (Thermo Fisher, #13–0700, 1:1,000), rabbit monoclonal anti-CREB1 (CST #9197, 1:1000), rabbit polyclonal anti-CREB5 (Immunoway, #YT7747, 1:1,000), rabbit monoclonal anti-CREB (phospho S133, Abcam #32096, 1:1,000), and rabbit monoclonal anti-PTEN (CST #9559, 1:1000). After the incubation with the above mentioned primary antibodies, membranes were incubated in corresponding horseradish peroxidase-conjugated secondary antibodies in 5 % milk-TBST and the protein bands were then developed with the Chemi-Doc Touch imaging system (Bio-Rad) and analyzed by the Image Lab software in the system. Tanon 2500 Gel Imaging System was also used for analysis of Western Blot results. Protein bands were analyzed and quantified by Quantity-One (Bio-Rad) or ImageJ with normalization by the corresponding loading controls in the same samples.

Indirect immunofluorescence

For immunofluorescence (IF) analysis of the mouse primary neurons, brain cortical tissues were firstly dissected from embryos of developmental stage at E15.5. The isolated neurons were cultured for two to three days in vitro. Cell number of 0.2×10^6 were seeded on a glass coverslip coated with poly-L-lysine and placed on 24-well plate for experiments. Cell fixation was performed by adding 4 % formaldehyde solution (in PBS) to the cells and incubated for 10–15 min and then in blocking solution with primary and secondary antibodies as described before [32]. Nucleus was counterstained with 4′,6-diamidino-2-phenylindole (DAPI) at concentration of 50 ng/ml for 15 min at room temperature. Microscopic images of the cells showing the localization and intensity of various fluorescent signals were analysis using a fluorescence microscope equipped with CCD cool-camera or with a confocal microscopy. Quantitative and statistical analyses were performed as described [30].

For IF staining in the brain tissues, mice were anesthetized and their brain tissues were subjected to fixation by 4 % paraformaldehyde (PFA) perfusion. The brains were then dissected and embedded in optimal cutting temperature compound with thickness of frozen sections of 10 μm, followed by permeabilization using 0.3 % Triton X-100, and incubation with the blocking buffer containing 5 % donkey serum at room temperature for one hour. After blocking, primary antibody was added to tissue sections which was incubated at 4 °C cold room overnight. Primary antibodies used in this study included rabbit polyclonal anti-Maf1 antibody (NOVUS, #31617, 1:200), mouse monoclonal anti-NeuN (Millipore, #MAB377, 1:200), mouse monoclonal anti-GFAP (Millipore, #MAB360,1:200), rabbit monoclonal anti-IBA-1 (Wako Chemicals, #019-19741,1:200), rabbit monoclonal anti-PSD-95 (CST# 3450, 1:200), rabbit monoclonal anti-Synaptophysin (CST #36406, 1:200), rabbit monoclonal anti-GAP43 (Signalway, #49013, 1:200), mouse monoclonal anti-NF160 (ThermoFisher, #13-0700, 1:200), chicken anti-beta-tubulin 3 (TUJ, AvesLabs, #TUJ-7947980, 1:200). Corresponding fluorescent-coupled secondary antibodies were then added to the samples and incubated for one hour at room temperature. Images were acquired in the peri-infarct area using fluorescence microscopy, and ImageJ was used for image processing and quantification. All experimental procedures and quantitative analyses were carried out by different investigators in blinded manner.

AAV-mediated Maf1 knockdown

AAV particles were established with a U6 promoter-driven shRNA expression system in AAV-PHP.eB vector (PackGene Biotech). Transduction efficiency was determined by an EGFP expression which was separately controlled by a CAG promoter. Maf1 shRNA was designed based on the target sequence of Maf1 specific 29mer shRNA which had been verified for efficient knockdown of Maf1 expression (OriGene TG516313). The plasmid was sequence-verified and transfected into HEK293 cells for viral particle packaging. All vectors were titered and analyzed by quantitative PCR. For the in vivo Maf1 knockdown experiments, AAV particles containing scramble or Maf1 shRNA were stereotaxically injected into the ipsilateral cortex at the coordination of M/L, 1.0 mm, 2.2 mm A/P, and 1.0 mm D/V for 21 days.

Behavioral assessment

Recovery of mice (n = 9–15 per group) after stroke was assessed by the grid-walk test, cylinder test, and adhesive removal test as described previously [37–39]. Baseline performance was measured a week before stroke surgery. These behavioral assessments were conducted once a week for 8 weeks. For grid-walk test, functional deficit was determined by the percentage of number of impaired (right limb) foot faults over the total step numbers on the grid. For performing the cylinder test, mice were placed in a one-liter volume glass beaker in a quiet room, and the contact times of the paw with the glass wall using the unimpaired paw, impaired paw and both paws were determined using a video-recorder with slow motion if necessary. The bias of paw use was determined by the difference between the fraction of the paw contact time spent on unimpaired limb and the impaired limb over the total time spent on unimpaired, impaired and simultaneous bilateral paws. The adhesive removal test was basically performed by measuring the time taken for the mice to remove the adhesive tapes from

Fig. 1. Pol III repression induced by mTORC1 inhibition is associated with Maf1 dephosphorylation and nuclear accumulation in mouse primary neurons. (A) Protein extracts prepared from mouse primary cortical neurons treated with or without 20 nM rapamycin (Rap) for 4 h and analyzed by Western blot (WB) analysis. (B) RT-PCR analysis of 5S precursor rRNA (pre-rRNA) and pre-$tRNA^{LEU}$ in cells from (A). Reactions without input (No DNA) and without reverse transcriptase (No RT) were served as controls. Right panel indicates quantification of transcription levels relative to untreated controls. Values of the data are expressed as mean and error bars represent ± SEM values, n = 6, $^{**}p < 0.05$, Mann-Whitney test. (C) RT-PCR analysis of 5S pre-rRNA and pre-$tRNA^{LEU}$ in primary cortical neurons treated with DMSO, 20 nM rapamycin or 1 μM PP242 for 4 h. Right panel indicates quantification of transcription levels relative to controls. Values of the data are expressed as mean and error bars represent ± SEM values, n = 6, $^{**}p < 0.05$, Mann-Whitney test. (D) Raptor knockdown by shRNA in primary cortical neurons was analyzed by WB using an antibody against Raptor. (E) RT-PCR analysis of 5S pre-rRNA level in primary cortical neurons transfected with scramble control or shRNA Raptor. Right panel indicates quantification of relative 5S pre-rRNA levels. Values of the data are expressed as mean and error bars represent ± SEM values, n = 6, $^{**}p < 0.05$, Mann-Whitney test. (F) Inhibition of mTORC1 leads to mobility shift of Maf1. Neuro2A cells expressing Myc-Maf1 were treated with 20 nM rapamycin for 30 min, and WB was used to analyze the Myc-Maf1 electrophoretic mobility shift with an antibody against Myc. Band 1 and 2 denote the fast and slow electrophoretic forms, respectively. (G) Inhibition of mTORC1 leads to dephosphorylation of Maf1. Primary cortical neurons were treated with 20 nM rapamycin or calf intestine alkaline phosphatase (CIP) for 30 min and WB was used to determine the mobility shift of Maf1 with anti-Maf1 antibody. (H) Immunofluorescence (IF) staining of Maf1 in primary cortical neurons which were treated in the absence or presence of 20 nM rapamycin for 4 h. Localization of Maf1 was analyzed by anti-Maf1 antibody. Cell and neurite morphology were visualized by beta-tubulin III staining. DAPI was used to counterstain the nucleus. Scale bar = 25 μm. Right panel indicates quantification of IF results showing Maf1 subcellular localization. Values of the data are expressed as mean and error bars represent ± SEM values, n = 6, $^{**}p < 0.05$, Mann-Whitney test.

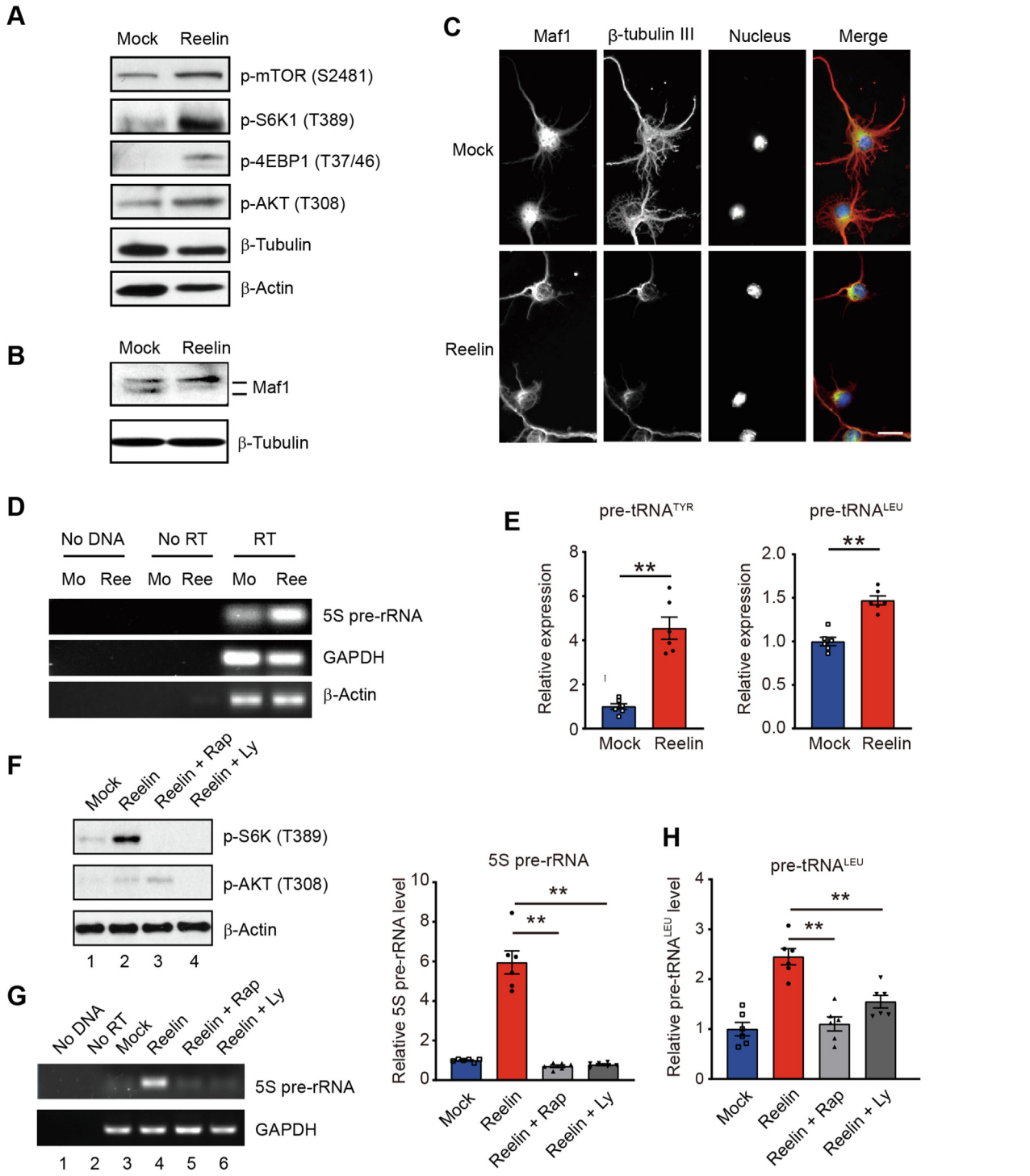

Fig. 2. Maf1 is phosphorylated and excluded from the nucleus which are accompanied by increased Pol III transcription after mTORC1 activation by Reelin in primary neurons. (A) WB analysis of mTOR signaling activity in primary cortical neurons incubated in Reelin- or the corresponding Mock-conditioned medium for 4 h. (B) Reelin stimulates Maf1 phosphorylation. Primary cortical neurons were incubated in Reelin- or the corresponding Mock-conditioned medium for 30 min. Electrophoretic analysis of Maf1 was performed by WB using an antibody against Maf1. (C) Maf1 localization in primary neurons incubated in Mock or Reelin-conditioned medium for 30 min. Maf1 was analyzed by immunofluorescence staining with a specific Maf1 antibody. Scale bar = 25 μm. (D) RT-PCR analysis of 5S pre-rRNA transcription in primary cortical neurons incubated in Mock or Reelin-conditioned medium for 4 h. (E) RT-qPCR analysis of $tRNA^{TYR}$ and $tRNA^{LEU}$ in primary cortical neurons incubated in Mock or Reelin-conditioned medium for 4 h. Values of the data are expressed as mean and error bars represent ± SEM values, n = 6, $^{**}p < 0.05$, Mann-Whitney test. (F) Reelin stimulation of mTOR signaling in primary cortical neurons is sensitive to rapamycin and Ly294002. Primary cortical neurons were pretreated 30 min with the indicated inhibitors, and then incubated in Reelin-conditioned medium containing the same drug for 20 min. mTOR signaling was analyzed by WB using p-S6K (T389) and p-AKT (T308) specific antibodies for mTORC1 and PI3K activity, respectively. (G) RT-PCR analysis of 5S pre-rRNA transcription. Right panel indicates quantification result. (H) RT-qPCR analysis of $tRNA^{LEU}$ transcription. Values of the data are expressed as mean and error bars represent ± SEM values, n = 6, $^{**}p < 0.05$, Mann-Whitney test.

their bilateral paws. Researchers were blinded to the animal identity during the analysis.

Golgi-Cox staining

After mice were anesthetized with isoflurane, brain tissues were quickly removed and washed with pre-chilled PBS, fixed with 4 % PFA, and cut into 2–3 mm sections based on the mouse brain atlas. Brain sections were first impregnated with mercuric chloride and potassium dichromate for seven days at room temperature, and subsequently in cryoprotective solution for four days before sectioning into 100 μm slices with a vibrating knife. The cut brain sections were placed on 0.3 % gelatin-pre-coated glass slides for dehydration in gradients by increasing concentrations of alcohol, followed by xylene. Brain slides were then sealed and developed. A Nikon microscope was used to acquire the images in the peri-infarct regions. ImageJ with the Simple Neurite Tracer plugin was used for Scholl analysis for the dendritic structures in the peri-infarct regions as described [40]. Dendritic spine density was determined by quantifying the number of protrusions per 10 μm dendritic branch.

BDA staining

Seven days before sample collection, 500 nl of 10 % biotinylated dextran amine (BDA) (wt/vol, Sigma) was stereotaxically injected to the same position of AAV injection site (1.0 mm A/P, 2.2 mm M/L, 1.0 mm D/V). After one week, mice were undergone the procedure of transcardial perfusion-fixation with 4 % PFA. BDA staining was determined by immuno-fluorescence microscopy with Streptavidin Alexa-flour 594. Image in the peri-infarct area was acquired by confocal microscopy. Three fields of view per mouse were obtained for quantification using ImageJ.

Cresyl violet staining

Brain tissues were removed after 4 % PFA perfusion-fixation as described above. The brain tissue blocks were dipped in wax, embedded and sectioned in 4 μm thickness. Xylene was then used to "de-wax" the brain sections, which was followed by re-hydration by decreasing concentrations of alcohol and Cresyl violet staining for 30 min at normal room temperature. After washing and dehydration, samples were transparentized and sealed with neutral gum. For measurement of the number of neuronal nucleolus in the peri-infarct region, three fields of view were randomly selected per section for quantification. Nissl body quantification was performed by the average optical density method (AOD = IOD/Area) and quantified by ImageJ. Cresyl violet staining was also used for quantification of infarct size after the PT stroke as reported previously [81].

Isolation of neurons from peri-infarct cortex

After PT stroke surgery, peri-infarct and the corresponding control tissues were collected by tissue punch and pooled from 6 mice per each experimental group. Adult Brain Dissociation Kit (BioWorthington) was used for dissociation and isolation of single cells from the bulk tissues based on the user menu. To remove the red blood cells from the samples, cell suspension was gone through the red blood cell removal step using the Red Blood Cell Lysis Solu-

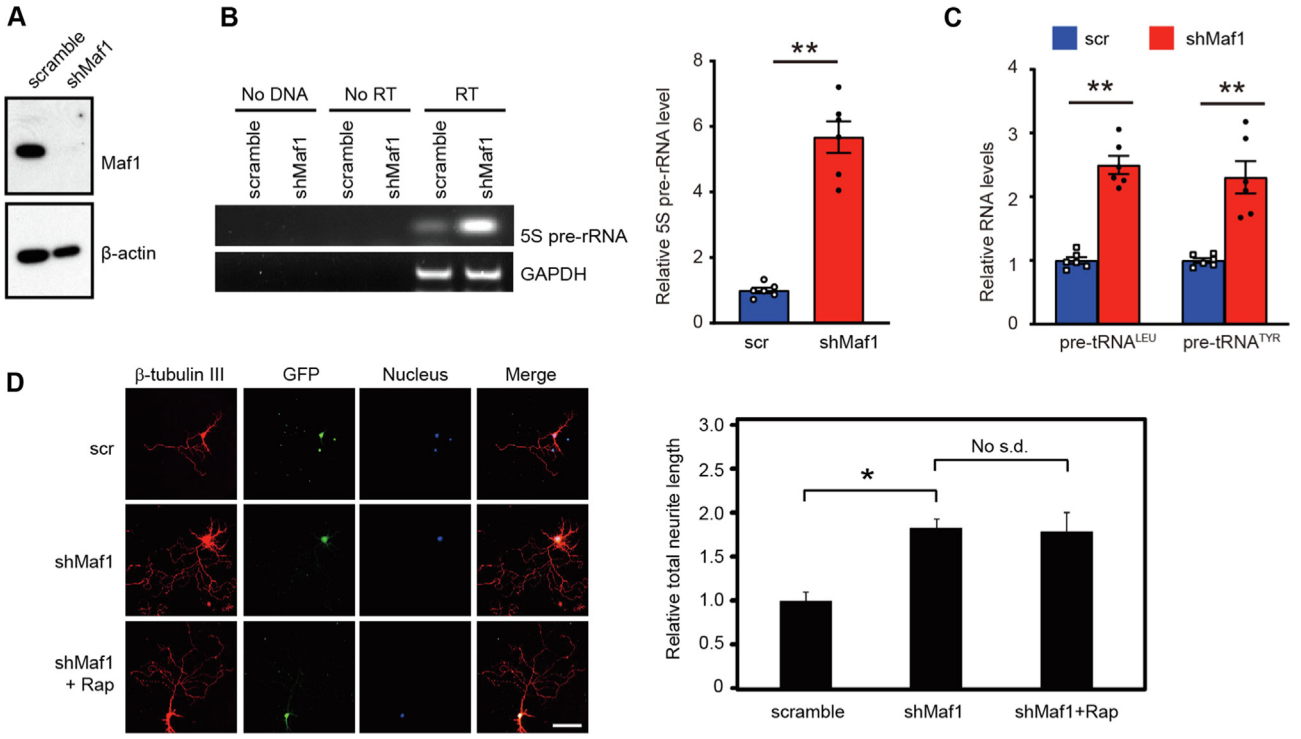

Fig. 3. Knockdown of Maf1 promotes Pol III-dependent transcription and neurite outgrowth. (A) Maf1 knockdown by shRNA was analyzed by WB using an antibody against Maf1 in primary cortical neurons transfected with a scramble or Maf1 shRNA. (B) RT-PCR analysis of 5S pre-rRNA expression in primary neurons after Maf1 knockdown as described in (A). Right panel indicates quantification result. Values of the data are expressed as mean and error bars represent ± SEM values, n = 6, $^{**}p < 0.01$, Mann-Whitney test. (C) RT-qPCR analysis of $tRNA^{LEU}$ and $tRNA^{TYR}$ in primary neurons after Maf1 knockdown as described in (A). Values of the data are expressed as mean and error bars represent ± SEM values, n = 6, $^{**}p < 0.01$, Mann-Whitney test. (D) IF analysis of neurites in primary neurons transfected with Maf1 shRNA and treated in the absence or presence of 20 nM rapamycin for 8 days. Transfected neurons were labeled by GFP. Neurite morphology was visualized by antibody against beta-tubulin III and DAPI was used to counterstain the nucleus. Right panel indicates quantification of total neurite length. Data are mean ± SEM of at least 50 randomly selected individual neurons per condition from 6 independent cultures. * $p < 0.05$ (Student's *t*-test). No significant difference (No s.d.). Scale bar = 50 μm.

tion (#130-094-183), and then Myelin Removal Beads II (Miltenyi Biotec catalog #130-096-731) was used for clearance of myelin fragments in samples. Neuronal cells were purified by the anti-biotin magnetic beads and LS columns provided in the Miltenyi MACS Neuron Isolation Kit (catalog #130-115-389).

CUT&Tag

We performed the Cleavage under targets and tagmentation (CUT&Tag) procedure according to the method described in the CUT&Tag Kit (Novoprotein Scientific, China, catalog #N259-YH01) with minor modifications as described previously [41,42]. Briefly, neurons were subjected to dead cell removal procedure following the instruction provided by the Dead Cell Removal Kit (MACS Miltenyi Biotec, catalog # 130-090-101), followed by a 5-min fixation with freshly prepared 1 % paraformaldehyde solution at room temperature, and then incubation for 5 min in 4 °C 125 mM glycine solution. Cells were subjected to gentle wash with Wash Buffer (20 mM HEPES at pH 7.5, NaCl at 250 mM, Spermidine at 0.5 mM, supplemented with protease inhibitor cocktails), and incubated with ConA beads in Antibody Buffer (NaCl at 150 mM, 20 mM HEPES at pH 7.5, Spermidine at 0.5 mM, 0.1 % BSA, 0.05 % Digitonin, 2 mM EDTA, protease inhibitor cocktail) together with the addition of corresponding antibodies as described in the user instruction. Primary antibodies used in this study included anti-Maf1 antibody (1:50 dilution, Novus #13617), normal rabbit IgG

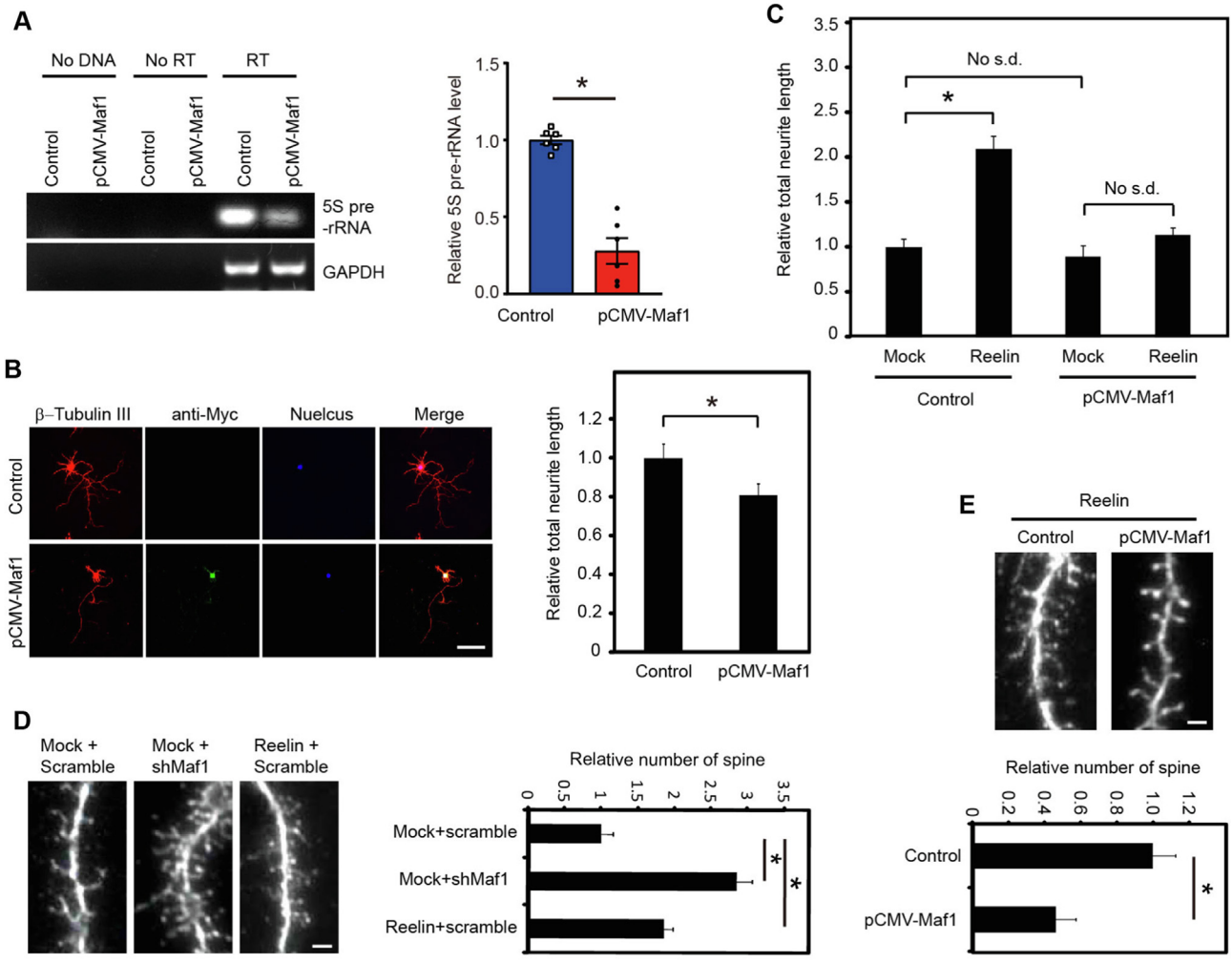

Fig. 4. Over-expression of Maf1 inhibits Pol III-dependent transcription, neurite outgrowth and dendritic spine growth in mouse primary neurons. (A) RT-PCR analysis of 5S pre-rRNA expression in primary cortical neurons transfected with pCMV-Myc-Maf1 or a control vector. Quantification results are shown in the right panel. Values of the data are expressed as mean and error bars represent ± SEM values, n = 6, $^*p < 0.05$, Mann-Whitney test. (B) IF analysis of neurites in primary neurons transfected with pCMV-Myc-Maf1 plasmid or control vector for 8 days. Red, beta-tubulin III; Green, Myc-Maf1; Blue, nucleus. Scale bar = 50 μm. Right panel indicates quantification of the relative total neurite length in neurons. Data are mean ± SD of at least 50 randomly selected individual neurons per condition from 6 independent cultures. $^*p < 0.05$ (Student's *t*-test). (C) Maf1 inhibits Reelin-induced neurite outgrowth. Primary cortical neurons were transfected with control vector or pCMV-Myc-Maf1 plasmid, followed by incubation in mock or Reelin-conditioned medium for 8 days, and relative total neurite length was measured compared with mock control. Data are mean ± SD of at least 50 randomly selected individual neurons per condition from 6 independent cultures. $^*p < 0.05$ (Student's *t*-test). No significant difference (No s.d.). (D) Representative images of dendritic spine morphology in primary neurons transfected with scramble or Maf1 shRNA, incubated in Mock or Reelin conditioned medium for 8 days and then analyzed by IF using beta-tubulin III. Scale bar = 5 μm. Right panel indicates quantification result. Data are mean ± SD of at least 50 prominent dendrites per condition from 6 independent cultures. $^*p < 0.05$ (Student's *t*-test). (E) Representative images of primary neurons transfected with control vector or pCMV-Myc-Maf1 plasmid and then incubated in Reelin-conditioned medium for 8 days. Spine morphology was analyzed by IF using beta-tubulin III antibody. Scale bar = 5 μm. Lower panel indicates quantification of the relative number of spine per dendrite length. Data are mean ± SD of at least 50 prominent dendrites per condition from 6 independent experiments. $^*p < 0.05$ (Student's *t*-test). (For interpretation of the references to color in this figure legend, the reader is referred to the web version of this article.)

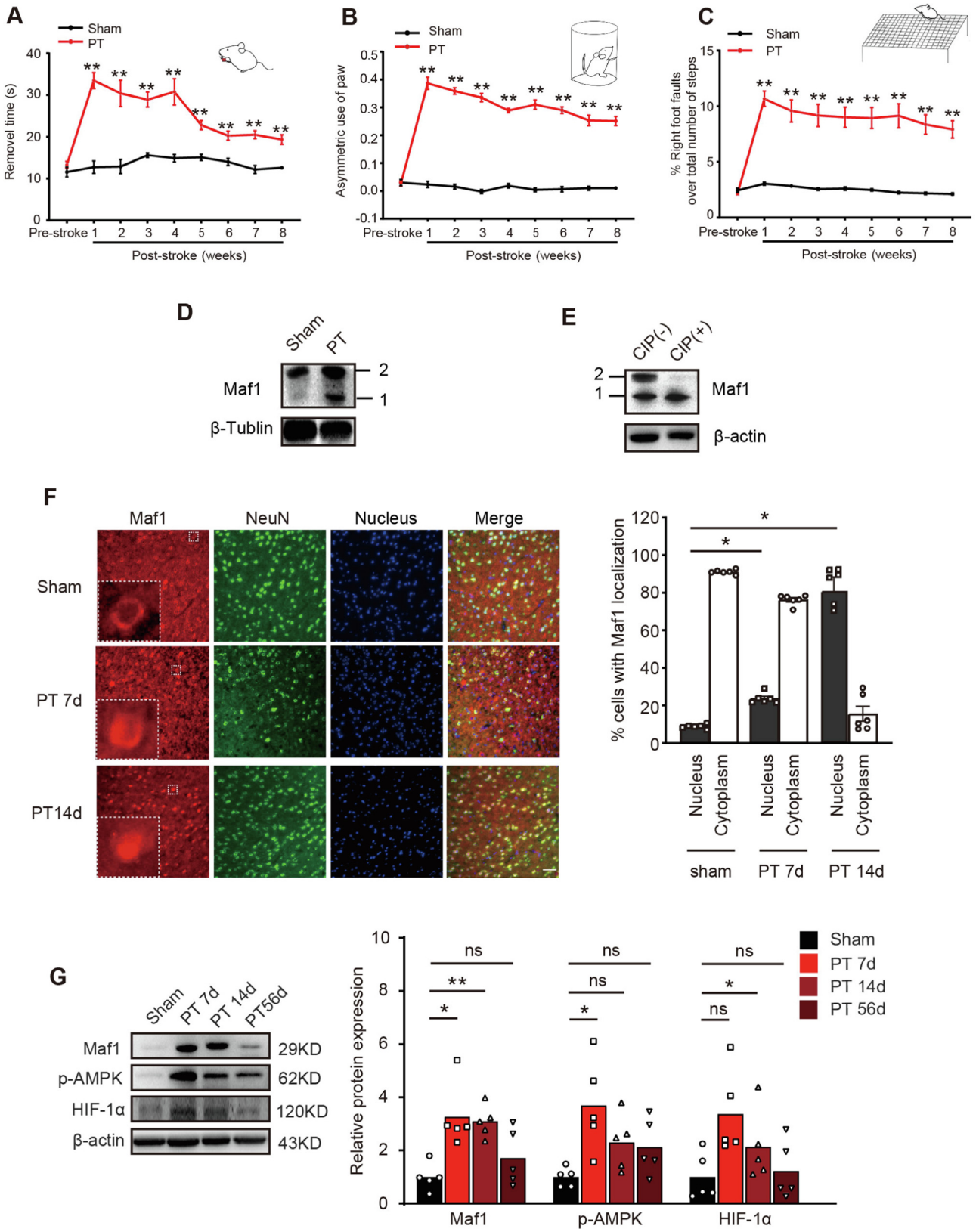
A
Sham
PT
Removel time (s)
Pre-stroke
Post-stroke (weeks)
B
Asymmetric use of paw
C
% Right foot faults over total number of steps
D
Sham
PT
Maf1
β-Tublin
E
CIP(-)
CIP(+)
Maf1
β-actin
F
Maf1
NeuN
Nucleus
Merge
Sham
PT 7d
PT14d
% cells with Maf1 localization
Nucleus
Cytoplasm
sham
PT 7d
PT 14d
G
Sham
PT 7d
PT 14d
PT56d
Maf1
p-AMPK
HIF-1α
β-actin
29KD
62KD
120KD
43KD
Relative protein expression
ns
PT 56d

(1:50 dilution, CST #2729), Rpb1 (1:100 dilution, CST#14958), and H3K27ac (1:200, CST#8173). After overnight incubation at 4 °C cold-room with gentle vertical rotation, the anti-rabbit IgG from goat (1:200 dilution, Ab6702, Abcam) diluted in Dig-wash buffer (20 mM HEPES at pH 7.5, Digitonin (0.05 %), NaCl (150 mM), Spermidine (0.5 mM), protease inhibitor cocktails) was added as the secondary antibody to enhance the signal and the cells were incubated at room temperature for one hour. Then, transposome treatment and tagmentation procedure were performed based on the user instruction. Treatment with proteinase K was performed at 50 °C for one hour. De-crossed linking of DNA was performed in 1 % SDS in the same buffer at 65 °C overnight. MinElute columns (Qiagen 28006) was used to purify DNA which was then subjected to PCR with the specific combination of indexed i5 and i7 primers in the master mix solution containing NEB Next HiFi 2x PCR reagents. The resulting DNA libraries were constructed using the following conditions. Step one: 72 °C for 5 min; step 2: 98 °C for 30 s; step 3: 12–25 cycles of 98 °C for 10 s; step 4: 63 °C for 30 s; step 5: 72 °C for 1 min for final extension. MinElute columns (Qiagen 28006) was used for purification of the library DNA. Quantification was measured by Qubit and the corresponding supersensitive detection reagents. Agilent Bioanalyzer was used for determining DNA fragment size. NovaSeq 6000 system (Illumina) was used for performing the pair-end DNA sequencing with a depth of 16 million reads by Novogene (Beijing, China). Standard Illumina software was used for data quality analysis in FASTQ files.

DATA processing and bioinformatics analysis

Trimming of the sequence reads was performed by PICARD. The resulting reads were then aligned to the mm10 mouse reference genome with Bowtie2 software package as described [43]. Peak calling was performed by MACS2 [44]. Differential binding peaks between peri-infarct neurons and control neurons were identified using MACS2 program. For visualization of the protein binding peaks, we used IGV genome browser [45]. HOMER package was used for peak annotation and motif analysis. For a comprehensive cluster analysis of genes and individual gene functions and pathway analysis, we used Gene Ontology (GO), Kyoto Encyclopedia of Genes and Genomes (KEGG) analysis for cluster and pathway analysis using DAVID bioinformatics resource [46,47]. Significant enrichments in GO terms and pathways were identified with *p*-value <0.05.

Statistical analysis

GraphPad Prism 8.01 software (GraphPad Software, Inc., CA) and Statistical Package For The Social Sciences (SPSS, version 27.0; SPSS Inc., Chicago) were used for statistical analyses in this study. For experiments with small sample size (n < 6), the corresponding p-values were determined by Mann-Whitney *U* test. Otherwise, Shapiro-Wilk test was used for normality analysis with a threshold of 0.05. and *p*-values were determined by Student's t-tests (two-tailed) or one-way ANOVA. P-values < 0.05 were regarded as statistical significance.

Results

Maf1 is regulated by mTORC1 in neurons

Maf1 is a conserved downstream effector of mTORC1 and is known as a repressor of Pol III transcription [12,48,49] in yeast and mammalian cells [9,10]. To ask whether mTORC1 controlled Pol III transcription in neuronal cells, we treated mouse primary cortical neurons with rapamycin, a selective inhibitor of mTORC1. Nascent transcripts of precursor 5S rRNA (5S pre-rRNA) and precursor $tRNA^{LEU}$ (pre-$tRNA^{LEU}$) were used to measure Pol III transcription rates [34,35]. We found that rapamycin inhibited mTORC1 activity as indicated by dephosphorylation of mTOR and its downstream substrates S6K1 and 4EBP1 (Fig. 1A), which were accompanied by marked repression of 5S rRNA and $tRNA^{LEU}$ genes (Fig. 1B) in neurons. Similar effect was observed in primary hippocampal neurons and Neuro2A cell line (Fig. S1). PP242, an ATP-competitive kinase inhibitor, exhibited similar activity to rapamycin toward inhibition of Pol III-dependent transcription (Fig. 1C). Moreover, knockdown of Raptor, an essential mTORC1 subunit, resulted in inhibition of 5S rRNA transcription (Fig. 1D-E). These results demonstrate that mTORC1 is a critical modulator of Pol III-dependent transcription in neuronal cells.

To determine whether Maf1 is regulated by mTORC1 in neurons, we expressed Myc-tagged Maf1 proteins in Neuro2A cells and measured the level of Maf1 phosphorylation by electrophoretic mobility shift analysis using anti-Myc antibody. It has been reported that Maf1 migrates in slow and fast electrophoretic forms which represent the phosphorylated/inactive form and dephosphorylated/active form of Maf1, respectively [9,50]. After rapamycin treatment, the slow electrophoretic form (band#2) disappeared and the fast form (band#1) became predominant (Fig. 1F). Similar Maf1 alteration was observed in primary cortical neurons (Fig. 1G). Moreover, we confirmed that the slow form disappeared after calf intestine phosphatase (CIP) treatment (Fig. 1G). Hence, these results indicate that inhibition of mTORC1 by rapamycin leads to Maf1 dephosphorylation and activation in cortical neurons.

It has been reported that mTORC1 suppresses Maf1 nuclear localization in yeast and MG63 cells [9,51]. To ask if Maf1 was regulated by mTOR similarly in neurons, we determined Maf1 subcellular localization by immunofluorescence (IF) staining. Under normal growth conditions, Maf1 is predominantly localized in the cytoplasm of primary hippocampal and cortical neurons. Upon rapamycin treatment, however, Maf1 became prominently accumulated in the nucleus (Fig. 1H & Fig. S2).

To further verify Maf1 regulation by mTOR in neuronal cells, we activated mTOR by Reelin as described previously [31,52] in cultured primary neurons. Consistently, we showed that Reelin treatment increased phosphorylation of mTOR, S6K1 and 4EBP1 (Fig. 2A). Importantly, Reelin treatment indeed promoted Maf1

Fig. 5. Characterization of Maf1 in the in vivo photothrombosis (PT) stroke model. (A-C) Spontaneous neurological recovery of the PT stroke model in a period of 8 weeks. Animals were induced with PT stroke or sham controls and neurological function was determined by adhesive removal test (A), cylinder test (B) and grid-walk test (C). Data in A-C are shown as mean ± SEM, n = 9 per group, ** $p < 0.01$ compared to the corresponding baseline time point (Pre-stroke) using repeated-measures ANOVA with Newman-Keuls multiple pairwise comparisons. (D) Mobility shift analysis of Maf1 in the peri-infarct cortex of PT mice or corresponding neurons in the sham control at day 7 post-stroke. Maf1 was detected by WB with an antibody against Maf1. Band 1 & 2 denote the fast and slow electrophoretic forms, respectively. (E) Treatment of the peri-infarct cortex of PT mice after 7 days of stroke induction with calf intestine alkaline phosphatase (CIP) for 30 min. Maf1 isoforms were detected by Western blot as described in (D). (F) Subcellular localization of Maf1 in the peri-infarct neurons at 7 and 14 days after PT stroke or the corresponding neurons in sham control. Maf1 and neurons were stained in red and green by co-immunofluorescence microscopy with Maf1 and NeuN antibodies, respectively. DAPI was used to counterstain the nucleus. Scale bar = 50 μm. Inserted images are magnified from the boxed neurons. Right panel indicates quantification result. Values of the data are expressed as mean and error bars represent ± SEM values, n = 6, * $p < 0.05$, ** $p < 0.01$, ANOVA with Newman-Keuls multiple pairwise comparisons. (G) Alteration of Maf1 protein expression in the peri-infarct cortex collected from sham, at the indicated time points after PT stroke mice. Maf1 expression was detected with Maf1 antibody by Western blot. Phosphor-AMPK (p-AMPK) and HIF-1α were used as the ischemic biomarker detected by Western blot. (For interpretation of the references to color in this figure legend, the reader is referred to the web version of this article.)

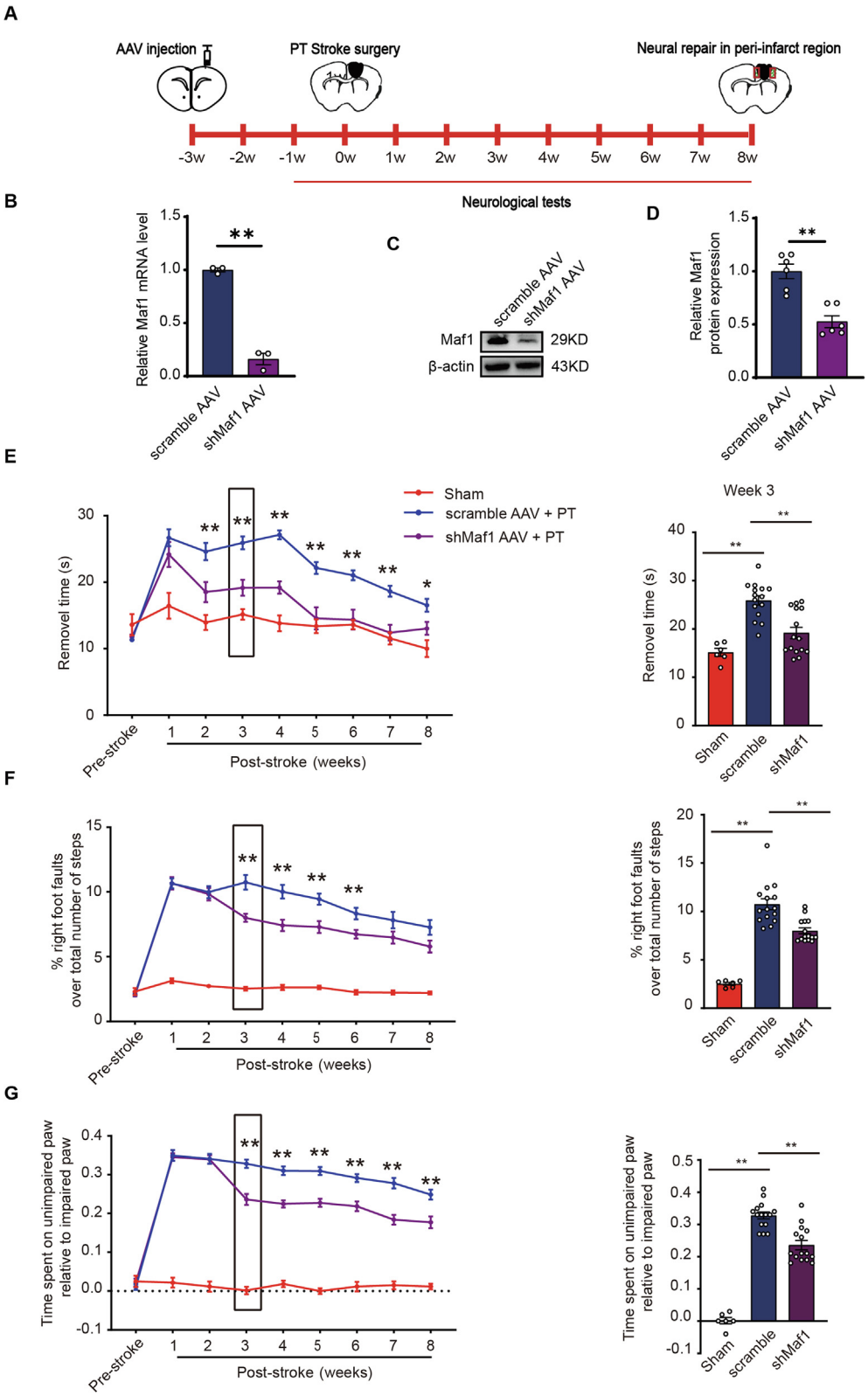

Fig. 6. Knockdown of Maf1 improves functional recovery in PT stroke model. (A) Timeline illustrates AAV-mediated knockdown of Maf1, PT stroke induction and behavior tests. (B) Verification of Maf1 knockdown by AAV expressing shRNA against Maf1. Mice were injected with shMaf1 or scramble AAV for 3 weeks, and the peri-infarct cortex were collected, and mRNA expression level of Maf1 was determined by RT-qPCR. Values of the data are expressed as mean and error bars represent ± SEM values, n = 3, $^{**}p < 0.01$, Mann-Whitney test. (C) Downregulation of Maf1 protein expression. peri-infarct cortex was collected as described in (B). WB was performed from the sample lysates for measurement of detection of Maf1 protein expression level with an antibody against Maf1. Beta-actin was used as loading control. (D) Quantification of Maf1 protein expression. Values of the data are expressed as mean and error bars represent ± SEM values, n = 6, $^{**}p < 0.01$, Mann-Whitney test. (E-G) Animals with Maf1 knockdown (shMaf1 AAV + PT) show improved motor functions during the indicated recovery period after PT stroke as determined by adhesive removal test (E), grid-walk test (F) and cylinder test (G). Right panels show the quantification of corresponding data at week 3 (boxed data) after stroke. Data in E-G are shown as mean ± SEM, n = 15 per group, $^{*}p < 0.05$, $^{**}p < 0.01$ using repeated-measures ANOVA with Newman-Keuls multiple pairwise comparisons.

phosphorylation (Fig. 2B) and exclusion from the nucleus (Fig. 2C), and enhanced 5S rRNA, $tRNA^{TYR}$ and $tRNA^{LEU}$ transcription (Fig. 2D-E). Pretreatment of primary cortical neurons with rapamycin blocked Reelin-induced mTORC1 activation (Fig. 2F) and transcription of 5S rRNA and tRNA (Fig. 2G-H). A similar effect was seen with the PI3K inhibitor Ly294002 in primary cortical neurons (Fig. 2F-H) and primary hippocampal neurons (Fig. S3). These results demonstrate that PI3K-mTORC1 signaling regulates phosphorylation, localization and transcription-repressing activity of Maf1 in neurons.

Maf1 is an intrinsic negative regulator of Pol III transcription and neurite outgrowth

To ask if Maf1 is a key regulator of Pol III transcription in neurons, we knocked down Maf1 and analyzed Pol III transcription in cultured mouse primary neurons. Maf1 knockdown led to significant increase in Pol III-transcribed 5S pre-rRNA and tRNAs (Fig. 3-A-C). Because Pol III transcription is key to the protein biosynthetic capacity of cells, we asked whether Maf1 regulates neurite growth, a process highly dependent on protein synthesis. In primary neurons after Maf1 knockdown, there was a robust increase in neurite outgrowth as revealed by IF staining with β-tubulin III, compared with control neurons (Fig. 3D). In addition, Maf1 knockdown-induced neurite outgrowth was blocked by rapamycin, indicating that Maf1 is the primary mediator of mTORC1-dependent neurite outgrowth (Fig. 3D).

To verify the suppressive role of Maf1 in neurite growth, we overexpressed Maf1 in primary neurons. As shown in Fig. 4A and 4B, Maf1 overexpression significantly repressed 5S rRNA transcription and neurite outgrowth. Maf1 overexpression also robustly attenuated Reelin-induced neurite outgrowth (Fig. 4C). Consistent with previous report [53], we showed that Reelin promoted dendritic spine formation (Fig. 4D, Fig. S3D). Remarkably, the effect on promoting spine formation by Maf1 knockdown was more robust than that by Reelin (Fig. 4D, Fig. S3D). Conversely, Maf1 overexpression blocked Reelin-induced spine density in primary neurons (Fig. 4E, Fig. S3E). Altogether, these observations suggest that Maf1 is an intrinsic suppressor of neurite outgrowth.

Characterization of Maf1 in peri-infarct neurons during spontaneous recovery after ischemic stroke in vivo

The observed suppressive effect of Maf1 on neurite outgrowth in vitro prompted us to examine its pathophysiological role in vivo. The mouse photothrombotic (PT) stroke model is widely used to investigate molecular and cellular events in spontaneous neurological recovery because limited neurite regeneration can be achieved in the peri-infarct cortex [5]. We used this model to induce focal sensorimotor cortical stroke (Fig. S4A). Blood perfusion imaging confirmed occluded cerebral blood flow (Fig. S4B) and the presence of infarct tissue (Fig. S4C–D). We used grid-walk, cylinder and adhesive removal tests to evaluate neurological deficits and the subsequent spontaneous recovery over 56 days after PT-induced stroke (Fig. 5A–C).

To characterize Maf1 during the spontaneous recovery period, we performed electrophoretic mobility analysis of Maf1 in the peri-infarct cortex collected at day 7 after PT-induced stroke. In sham control, Maf1 was mostly in phosphorylated form (Fig. 5D, band #2). In contrast, substantial fraction of Maf1 became dephosphorylated form after PT stroke (Fig. 5D, band #1) or CIP treatment (Fig. 5E, band #1). Immunofluorescence staining showed that Maf1 was predominantly in the cytoplasm of sham control neurons, whereas more neurons showed prominent Maf1 nuclear accumulation at day 7 and 14 after stroke (Figs. 5F, S5D–E). Overall Maf1 protein expression was prominently upregulated during the first 2 weeks after stroke in the peri-infarct cortex compared with sham control, but returned to basal level at day 56 (Fig. 5G). At day 7 and day 14, the peri-infarct cortex was ischemic as indicated by increased expression of p-AMPK and HIF-1α markers for glucose-deprivation and hypoxia, respectively (Fig. 5G). These observations suggest that Maf1 is an intrinsic neurite outgrowth suppressor by repressing the growth-associated Pol III transcription in the ischemic peri-infarct neurons during spontaneous recovery after stroke.

Knockdown of Maf1 promotes spontaneous recovery and neural repair

To determine the role of Maf1 in post-stroke spontaneous repair and recovery, we knocked down Maf1 by an AAV vector co-expressing GFP and Maf1 specific shRNA in the sensorimotor cortex of mouse brains (Fig. 6A). Majority of GFP^+ cells were overlapped with $NeuN^+$ cells (56.5 %), whereas only minor GFP^+ cell populations were $GFAP^+$ (9.2 %) and $IBA1^+$ (12.7 %) (Fig. S5), indicating that this AAV serotype prefers neurons as reported previously [54,55]. We further confirmed that AAV-mediated knockdown in cortical tissue led to significant reduction of Maf1 expression at both mRNA and protein levels (Fig. 6B–D).

We next evaluated the effect of Maf1 knockdown on spontaneous neurological recovery during a period of 8 weeks. Intriguingly, results from adhesive removal, cylinder and grid-walk assays all indicated that Maf1 knockdown significantly improved the neurological performance compared with the AAV scramble shRNA control (Fig. 6E–G). At the end of the study period, the mice were sacrificed and their brain sections and peri-infarct cortical tissues were collected for evaluation of structural neural repair. The expression of the presynaptic neurofilament marker NF-160 and the postsynaptic marker PSD95 were significantly enhanced in Maf1 knockdown mice compared with controls as evidenced by RT-qPCR (Fig. 7A, 7D), Western Blot analysis (Fig. 7B, 7E), and IF staining (Fig. 7C, 7F). To corroborate these observations, we analyzed the dendritic spine morphology and dendritic branching by Golgi-Cox staining. Maf1 knockdown significantly increased the density of dendritic spines in the peri-infarct neurons (Fig. 7G and Fig. S6G). The dendritic branch was more complex in the Maf1-knocked down peri-infarct neurons compared with that in control (Fig. 7H–I). BDA-immunostaining showed that Maf1 knockdown significantly enhanced axon regeneration (Fig. 7J). Maf1 knockdown did not significantly change the cerebral infarct size (Fig. S6A–B), density of neurons (Fig. S6C–D, S6F) and apoptotic cells (Fig. S6E) in the peri-infarct cortex.

We further examined whether Maf1 knockdown influenced the nucleolus, a nuclear organelle for ribosome biogenesis [56]. The percentage of neurons showing more nucleoli (≥3 per nucleus) in the peri-infarct cortex in the Maf1 knockdown group was significantly higher than that in the scramble control group (Fig. 7K). Nissl body abundance in neurons reflects the cellular protein synthetic capacity, and has been associated with regenerative ability in CNS neurons after injury (58). Maf1 knockdown significantly enhanced the mean density of Nissl body in the peri-infarct neurons compared with control (Fig. 7L). Hence, knockdown of Maf1 de-represses Pol III transcribed 5S rRNA and tRNAs, enhancing ribosome biogenesis, protein synthesis and neurite regrowth capacity of neurons. Taken together, these findings demonstrate

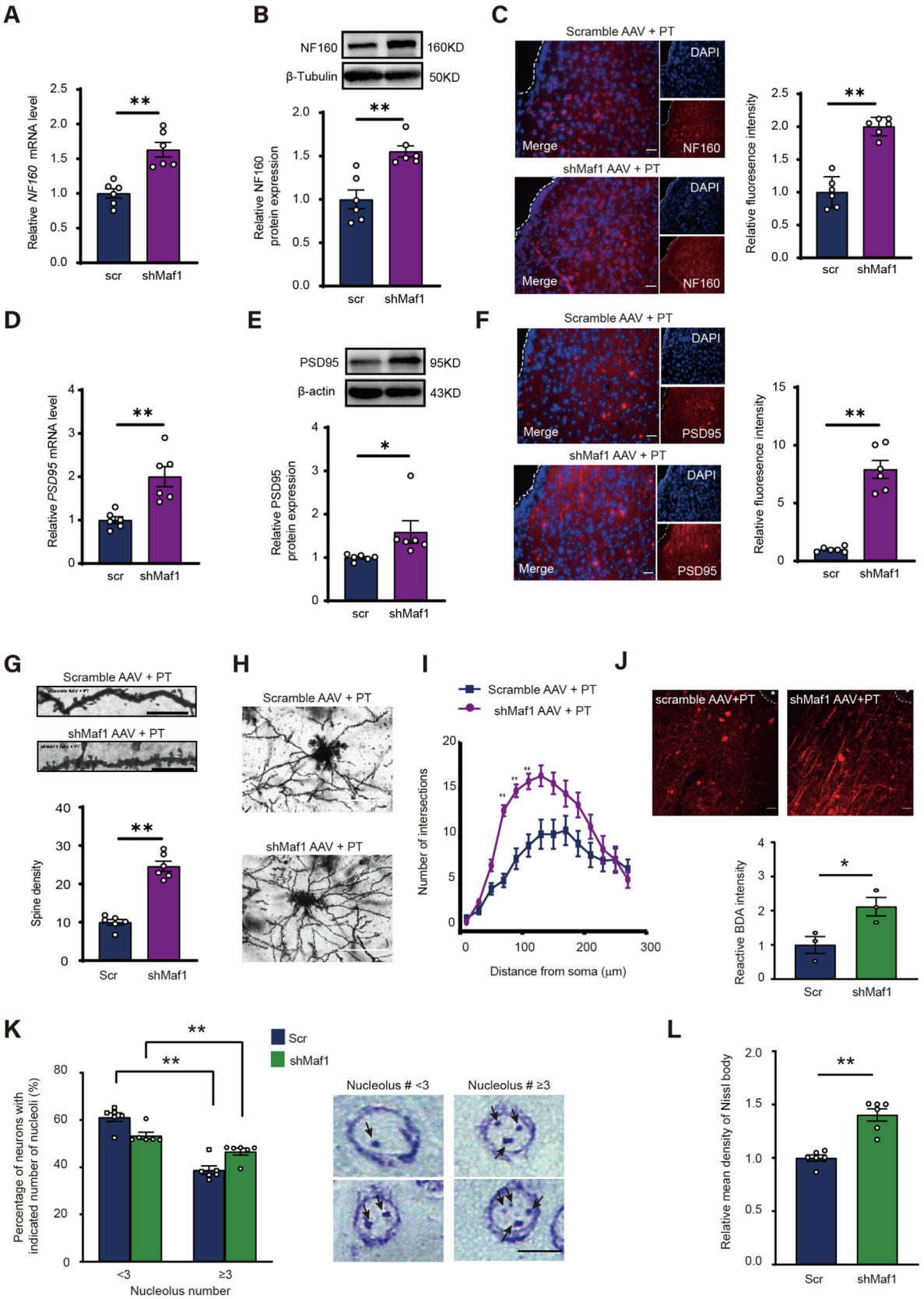
A
Relative NF160 mRNA level
scr
shMaf1
B
NF160
160KD
β-Tubulin
50KD
Relative NF160 protein expression
C
Scramble AAV + PT
shMaf1 AAV + PT
DAPI
Merge
NF160
Relative fluoresence intensity
D
Relative PSD95 mRNA level
E
PSD95
95KD
β-actin
43KD
Relative PSD95 protein expression
F
PSD95
G
Spine density
Scr
H
I
Number of intersections
Distance from soma (μm)
J
scramble AAV+PT
shMaf1 AAV+PT
Reactive BDA intensity
K
Percentage of neurons with indicated number of nucleoli (%)
Nucleolus number
Nucleolus # <3
Nucleolus # ≥3
L
Relative mean density of Nissl body

that Maf1 knockdown significantly promotes neural repair and neurological recovery after stroke.

Maf1 suppresses spontaneous recovery through repression of Pol III and CREB-associated genes in peri-infarct neurons in vivo

Apart from Pol III, recent evidence has shown that Maf1 also regulates Pol II-dependent transcription [19–21]. Given that transcriptional reprogramming is involved and plays a crucial role in neural repair after CNS injury [58], we sought to carry out a comprehensive analysis of Maf1 target genes by mapping the whole-genome chromatin-binding sites of Maf1 in the peri-infarct neurons in the PT stroke model. To this end, we isolated neuronal cells from the peri-infarct cortex at day 7 post-stroke, and mapped the genome-wide Maf1 chromatin binding sites using modified CUT&Tag approach according to our previous study [42]. To validate the results, we profiled Rpb1 (RNA polymerase II core subunit) binding and H3K27ac (active transcription marker) in isolated peri-infarct neurons and control neurons. As shown in Fig. 8A, Rpb1 and H3K27ac peaks were enriched at the promoter of the transcriptionally active house-keeping genes *GAPDH* and *ACTB*, demonstrating the quality of our CUT&Tag results. Bioinformatics analysis identified the genes with differential Maf1 binding at the promoter regions, 52.68 % of which were upregulated in the peri-infarct neurons compared with control neurons, whereas 41.62 % was downregulated (Fig. 8B, Table S1). In agreement with our earlier results, Maf1-binding was upregulated in Pol III-transcribed 5S rRNA and tRNA genes in peri-infarct neurons (Fig. 8D, Table S2), supporting the idea that the elevated Maf1 represses Pol III-transcribed genes, restraining ribosome biogenesis, protein biosynthetic capacity and neurite regeneration necessary for neural repair.

In addition to Pol III genes, we identified many Maf1 binding peaks at promoters of Pol II-transcribed genes. As shown in Fig. 8C, HOMER analysis of Maf1 binding motifs specific to the peri-infarct neurons showed that the most matched motif was cyclic AMP response element binding protein (CREB). We further performed MACS2 differential binding analysis. The results showed that CREB-related genes with upregulated Maf1 binding included CREB1, CREB5, CREBL2, CRTC3, ATF4 and the epigenetic modifier SRCAP (Fig. 8E, Table S1). Interestingly, Gene Ontology-Cellular Component Analysis further showed that many genes with upregulated Maf1 binding encode cytoskeleton and microtubule proteins, which are closely associated with neurite regeneration and synaptic plasticity.

To verify whether Maf1 binding is required for transcriptional repression of these genes, we knocked down Maf1 in the peri-infarct cortex and determined the change of expression of these genes at day 7 after stroke. We found that Maf1 knockdown significantly enhanced the expression of CREB1 and CREB5 in both mRNA level and protein level (Fig. 8F-I). Moreover, Maf1 knockdown resulted in significant increase in the level of p-CREB (S133) (Fig. 8J), the transcriptionally active CREB1 form [59]. Similar results were observed in peri-infarct cortex collected at day 14 after stroke (Fig. S7A–E). Consistently, Maf1 knockdown also elevated the expression of brain derived neurotrophic factor (BDNF), which is a known target gene of CREB1, in the peri-infarct cortex at the corresponding time points after stroke (Fig. 8K & Fig. S8). In addition, knockdown of Maf1 resulted in upregulation of Pol III-transcribed 5S rRNA and tRNA genes (Figs. 8L–M, S7F–H). Overall, these results demonstrate that Maf1 binds to and represses Pol III- and CREB-associated genes that are important for neural repair during spontaneous recovery after stroke.

Discussion

In this report, we demonstrate that Maf1 is a novel intrinsic suppressor of spontaneous recovery by regulating transcriptional reprogramming in the peri-infarct neurons of the experimental stroke model. Mechanistically, Maf1 not only represses its canonical targets of Pol III-transcribed genes (e.g. tRNA and 5S rRNA genes), but also represses Pol II-transcribed CREB and CREB-target genes in the peri-infarct neurons during the post-stroke spontaneous recovery time frame. Collectively, these Pol II and Pol III transcribed genes become derepressed after Maf1 knockdown, promoting regrowth of axons/dendrites and synaptic plasticity. Importantly, the structural improvement due to neural repair leads to enhanced functional neurological recovery. Thus, these results suggest that Maf1 is a potential drug target for potentiating neural repair and recovery after ischemic stroke.

RNA Polymerase III activity is a critical determining factor for cell growth [60,61]. In this study, we demonstrated that Maf1 plays a critical role in Pol III repression by targeting the promoters of 5S rRNA and tRNA genes in the nervous system. Maf1 expression, dephosphorylation, nuclear localization and binding to Pol III target promoters are all up-regulated in the peri-infarct neurons. Maf1 knockdown leads to elevated transcription of these genes,

Fig. 7. Knockdown of Maf1 enhances synaptic plasticity after PT stroke. (A) At day 56 after PT stroke as described in Fig. 6, peri-infarct cortical tissues from the brains of mice with scramble or Maf1 shRNA AAV injection were collected for RT-qPCR detection of NF160 mRNA expression level. Values of the data are expressed as mean and error bars represent ± SEM values, n = 6, $^{**}p < 0.01$, Mann-Whitney test. (B) Brain samples were collected as described in (A) and WB was performed for determination of NF160 protein expression. Values of the data are expressed as mean and error bars represent ± SEM values, n = 6, $^{**}p < 0.01$, Mann-Whitney test. (C) Brain sections were collected from the experimental mice described in (A). NF160 expression in the peri-infarct region was determined by immunofluorescence staining using anti-NF160 antibody. White dotted line denotes that boundary of infarct region. Scale bar = 50 μm. Values of the data are expressed as mean and error bars represent ± SEM values, n = 6, $^{**}p < 0.01$, Mann-Whitney test. (D) Brain samples were collected for detection of PSD95 mRNA expression by RT-qPCR. Values of the data are expressed as mean and error bars represent ± SEM values, n = 6, $^{**}p < 0.01$, Mann-Whitney test. (E) Brain samples were collected and WB was performed to determine the PSD95 protein expression. Values of the data are expressed as mean and error bars represent ± SEM values, n = 6, $^{**}p < 0.01$, Mann-Whitney test. (C) Brain sections were collected from the experimental mice described in (A). PSD95 expression in the peri-infarct region was determined by immunofluorescence staining using anti-PSD95 antibody. White dotted line denotes that boundary of infarct region. Scale bar = 50 μm. Values of the data are expressed as mean and error bars represent ± SEM values, n = 6, $^{**}p < 0.01$, Mann-Whitney test. (G) Knockdown of Maf1 increases dendritic spine density in the peri-infarct neurons. Golgi-Cox staining shows the dendritic spine density in scramble (upper panel) and Maf1 knockdown brains (lower panel). Scale bar = 50 μm. Values of the data are expressed as mean and error bars represent ± SEM values, n = 6, $^{**}p < 0.01$, Mann-Whitney test. (H) Knockdown of Maf1 increases dendritic complexity in the peri-infarct neurons. Golgi-Cox staining shows the representative dendritic morphology in scramble (upper panel) and Maf1 knockdown brains (lower panel). Scale bar = 50 μm. (I) Sholl analysis showing the number of dendritic intersections in the Golgi-Cox staining in (H). Scale bar = 50 μm. Values of the data are expressed as mean and error bars represent ± SEM values, n = 6, $^{**}p < 0.01$, Mann-Whitney test. (J) Knockdown of Maf1 increases promotes axon growth in the peri-infarct neurons. Axons in the peri-infarct region of scramble and Maf1 knockdown (shMaf1) AAV injected brains were labelled with BDA and detected by immunofluorescence imaging. Scale bar = 20 μm. Lower panel shows the quantification result. Values of the data are expressed as mean and error bars represent ± SEM values, n = 3, $^{*}p < 0.05$, Mann-Whitney test. (K) The nucleolar numbers in the peri-infarct neurons in scramble and Maf1 knockdown mice at day 56 after stroke. Values of the data are expressed as mean and error bars represent ± SEM values, n = 6, $^{**}p < 0.01$, Mann-Whitney test. Images show the nucleolar numbers in the peri-infarct neurons detected by Nissl staining. Arrows indicate nucleoli. Scale bar = 50 μm. (L) Quantification of the relative density of Nissl body detected by Nissl staining in the peri-infarct neurons in sham and Maf1 knockdown mice. Values of the data are expressed as mean and error bars represent ± SEM values, n = 6, $^{**}p < 0.01$, Mann-Whitney test.

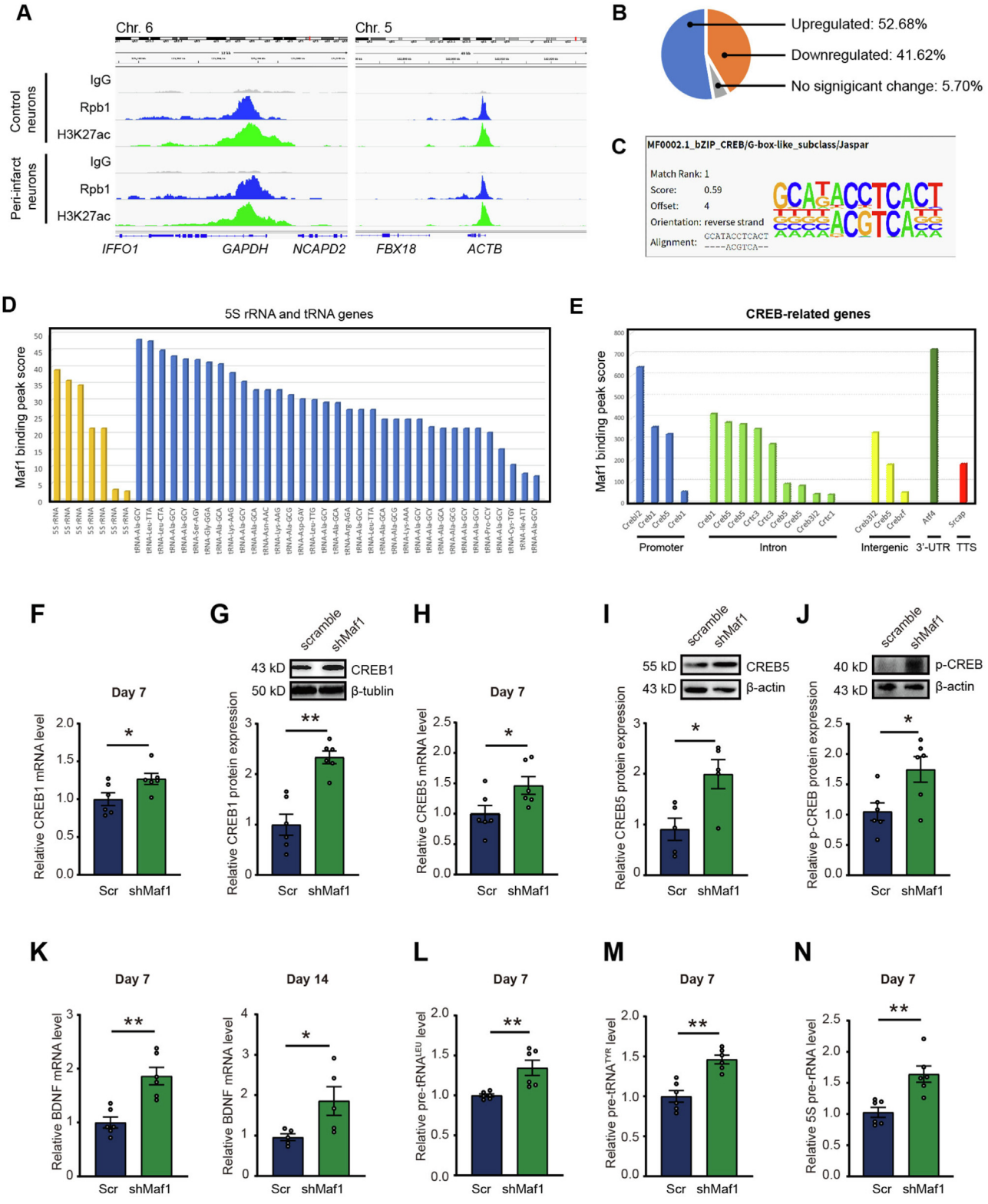
A
Chr. 6
Chr. 5
Control neurons
Peri-infarct neurons
IgG
Rpb1
H3K27ac
IFFO1
GAPDH
NCAPD2
FBX18
ACTB
B
Upregulated: 52.68%
Downregulated: 41.62%
No signigicant change: 5.70%
C
MF0002.1_bZIP_CREB/G-box-like_subclass/Jaspar
Match Rank: 1
Score: 0.59
Offset: 4
Orientation: reverse strand
Alignment: GCATACCTCACT ----ACGTCA--
D
5S rRNA and tRNA genes
Maf1 binding peak score
E
CREB-related genes
Maf1 binding peak score
Promoter
Intron
Intergenic
3'-UTR
TTS
F
Day 7
Relative CREB1 mRNA level
Scr
shMaf1
G
scramble
shMaf1
43 kD
CREB1
50 kD
β-tublin
Relative CREB1 protein expression
H
Day 7
Relative CREB5 mRNA level
I
scramble
shMaf1
55 kD
CREB5
43 kD
β-actin
Relative CREB5 protein expression
J
scramble
shMaf1
40 kD
p-CREB
43 kD
β-actin
Relative p-CREB protein expression
K
Day 7
Relative BDNF mRNA level
Day 14
Relative BDNF mRNA level
L
Day 7
Relative pre-tRNA^LEU level
M
Day 7
Relative pre-tRNA^TYR level
N
Day 7
Relative 5S pre-rRNA level

which is accompanied by higher capacity of ribosome biogenesis and protein synthesis as indicated by nucleolar number and Nissl body staining, respectively, in the peri-infarct cortex. Because protein biosynthetic components (e.g. tRNAs and ribosomes) play important role in CNS axon regeneration [57], it is reasonable to propose that Maf1 suppresses neural repair and functional recovery through inhibition of RNA polymerase III-dependent transcription. In addition to dephosphorylation and nuclear accumulation, Maf1 expression is upregulated during the critical recovery period after focal ischemic stroke in the peri-infarct cortex, which could provide a sustaining inhibitory effect on functional recovery. Future work will be required to elucidate if Maf1 expression is regulated by mTORC1 or another mechanism.

Maf1 is commonly known as a Pol III repressor. Recent evidence suggests that Maf1 also acts on Pol II-transcribed gene [19–21]. The current study reveals that CREB-associated genes are Maf1 targets during spontaneous recovery after stroke. The bZIP transcription factor CREB is known to promote consolidation of memory through enhancing neuronal excitability and nerve plasticity in the brain [62]. It has also been reported that CREB modulates neurite regeneration in CNS and PNS neurons [63,64]. After dorsal column lesion, viral transduction of active CREB leads to robust regeneration of axons in the dorsal root ganglions [65]. Virus-mediated CREB overexpression in the motor cortex also enhances recovery of motor deficit after stroke [66]. However, CREB activation is absent from the brain during spontaneous recovery after stroke [67], which may be due to Maf1 repression based on the findings in this study as Maf1 knockdown elevates CREB expression and activity. CREB-target genes are involved in axon guidance, growth cone extension, neural plasticity, cytoskeleton rearrangement and neural network reconnection [65,66]. Therefore, the coordinated expression of these genes is likely to mediate Maf1 knockdown-induced neural repair and recovery of neurological functions after stroke and other CNS injury.

In line with our findings, a recent report in cultured hippocampal neurons has indicated that Maf1 negatively regulates dendritic morphogenesis, and knockdown of Maf1 in normal adult mice increases synaptogenesis in the hippocampus in vivo which is accompanied by enhanced performance of learning and memory [68]. The same group further used an optic nerve injury model in adult mice to demonstrate that knockdown of Maf1 promotes axon regeneration of retinal ganglion cells [69]. However, the downstream effector regulated by Maf1 for the observed cellular responses in these contexts remains unclear. It would be interesting to examine whether Maf1-mediated transcriptional regulation also plays an important role in these scenarios.

mTOR signaling has recently emerged as a key regenerative pathway after CNS injury. Several studies demonstrated that loss of PTEN, a major upstream negative regulator in mTOR pathway, stimulates repair and axonal regeneration of both injured CNS and peripheral nerves [70–72]. However, it should be noted that PTEN is a key tumor suppressor and somatic mutation of PTEN is frequently observed in various types of cancers. PTEN ablation results in tumor development in multiple tissues in animal models, including brain cancers [73,74]. In contrast, Maf1 is a downstream effector of mTORC1 and ablation of Maf1 can also potentiate neural repair processes as demonstrated in this study. Unlike PTEN knockout, Maf1 knockout is not tumorigenic but even provides resistance to diet-induced fatty liver and obesity [75]. Since the PT stroke model is specifically used for axon regeneration and neural repair research owing to the lack of penumbra, we cannot rule out the possibility that Maf1 may also have neuroprotective effect after stroke. We are currently using MCAO stroke model to address this question.

With respect to the potential clinical translation of targeting Maf1, recent new technologies such as DNA framework drug delivery systems [76–79] and RNA-based therapeutic strategies [80] have shown promising potential to silence specific gene targets for injury treatment and promoting neural repair in PNS and CNS. These drug delivery systems can be delicately designed into specific spatial structures for targeting diverse drugs such as small molecule inhibitors, RNAi or peptides to facilitate the target-specific delivery of cargo for downregulation of gene expression. Moreover, some of them such as the tetrahedral framework nucleic acids even possess excellent biocompatibility feature and various neuroprotective and angiogenesis-promoting effects *per se* [76,78]. It would be interesting to examine their translational application in neural repair after stroke in future studies.

Conclusion

The present study demonstrates that Maf1 is an intrinsic neural repair suppressor against regenerative capability of mature CNS neurons, suggesting that Maf1 is a novel therapeutic target for potentiating neural plasticity and functional recovery after stroke and other CNS injuries.

Compliance with ethics requirements

All Institutional and National Guidelines for the care and use of animals (fisheries) were followed.

Fig. 8. Elevated Maf1 binding to Pol-III and neuroplasticity-related genes in peri-infarct neurons. (A) Magnetic column-isolated adult neurons from per-infarct tissues of PT stroke at day 7 or from control mice were subjected to CUT&Tag-Seq analysis. IGV genome browser showing that CUT&Tag-binding profiles of IgG (background control), Rpb1 (RNA polymerase II subunit), and acetylated H3K27 (ac-H3K27) at the genomic regions of the representative GAPDH (left) and ACTB (right) in control and peri-infarct neurons. (B) Pie chart showing the numbers of upregulated Maf1-binding peaks (943 peaks, indicated in blue color), down-regulated peaks (745 peaks, indicated in red color) and peaks without significant change (102 peaks, indicated in gray color) in peri-infarct neurons compared with control neurons. (C) Homer motif enrichment analysis against Maf1-binding sequences in the peri-infarct neurons indicate CREB binding motif is the best match. (D) Differentially upregulated gene expression of 5S rRNA (orange) and tRNAs (blue) in the peri-infarct neurons compared with control neurons. Differential binding peaks and annotations were identified by MACS2. (E) Differentially upregulated Maf1 binding to the promoter of CREB-related genes in the peri-infarct neurons compared with control neurons. Differential binding peaks and annotations were identified by MACS2. (F) Knockdown of Maf1 enhances CREB expression and activity in the peri-infarct cortex. (F, H) Mice were injected with shMaf1 or scramble AAV for 3 weeks, and subjected to PT stroke for 7 days. The peri-infarct cortex was then collected and CREB1 and CREB5 mRNA expression levels was determined by RT-qPCR. Values of the data are expressed as mean and error bars represent ± SEM values, n = 6, * $p < 0.05$, Mann-Whitney test. (G, I) Samples were collected as described in (A) and protein lysates were prepared for analysis of protein expression of CREB1 and CREB5 by Western blot. Right panels show quantification results. Values of the data are expressed as mean and error bars represent ± SEM values, n = 6, ** $p < 0.01$, Mann-Whitney test. (J) Knockdown of Maf1 promotes CREB activity in the peri-infarct cortex. Protein samples were collected as described in (B) and CREB1 activity was determined by phosphorylation at serine residue S133 using the specific anti-p-CREB (S133) antibody by Western blot. Values of the data are expressed as mean and error bars represent ± SEM values, n = 6, * $p < 0.05$, Mann-Whitney test. (K) Knockdown of Maf1 promotes CREB-target gene expression. RNA samples were collected as described in (A) at day 7 and day 14 after stroke, and BDNF mRNA expression was determined by RT-qPCR. Values of the data are expressed as mean and error bars represent ± SEM values, n = 6, *$p < 0.05$, **$p < 0.01$, Mann-Whitney test. (L-N) RNA samples were collected as described in (A) and expression of pre-tRNA^{LEU} (L), pre-tRNA^{TYR} (M) and 5S pre-rRNA (N) was determined by RT-qPCR. Values of the data are expressed as mean and error bars represent ± SEM values, n = 6, **$p < 0.01$, Mann-Whitney test. (For interpretation of the references to color in this figure legend, the reader is referred to the web version of this article.)

Declaration of Competing Interest

The authors declare that they have no known competing financial interests or personal relationships that could have appeared to influence the work reported in this paper.

Acknowledgements

This work was financially supported by the research grants including the National Natural Science Foundation of China (grant # 81974210), the Science and Technology Planning Project of Guangdong Province (grant # 2020A0505100045), the Natural Science Foundation of Guangdong Province (grant # 2019A1515010671), and the New Jersey Commission on Brain Injury Research (grant # CBIR11PIL033). We thank Prof. Jin-Moo Lee and Dr. Zach Rosenthal for technical advice concerning the photothrombotic stroke model.

Appendix A. Supplementary material

Supplementary data to this article can be found online at https://doi.org/10.1016/j.jare.2022.11.007.

References

[1] Feigin VL, Stark BA, Johnson CO, Roth GA, Bisignano C, Abady GG, et al. Global, regional, and national burden of stroke and its risk factors, 1990–2019: a systematic analysis for the Global Burden of Disease Study 2019. Lancet Neurol 2021;20(10):795–820.
[2] Wang YJ, Li ZX, Gu HQ, Zhai Y, Jiang Y, Zhao XQ, et al. China Stroke Statistics 2019: a report from the National Center for Healthcare Quality Management in Neurological Diseases, China National Clinical Research Center for Neurological Diseases, the Chinese Stroke Association, National Center for Chronic and Non-communicable Disease Control and Prevention, Chinese Center for Disease Control and Prevention and Institute for Global Neuroscience and Stroke Collaborations. Stroke Vasc Neurol 2020;5(3):211–39.
[3] Powers WJ, Rabinstein AA, Ackerson T, Adeoye OM, Bambakidis NC, Becker K, et al. 2018 Guidelines for the early management of patients with acute ischemic stroke: a guideline for healthcare professionals from the American Heart Association/American Stroke Association. Stroke 2018.
[4] Cramer SC. Treatments to promote neural repair after stroke. J Stroke 2018;20(1):57–70.
[5] Carmichael ST, Kathirvelu B, Schweppe CA, Nie EH. Molecular, cellular and functional events in axonal sprouting after stroke. Exp Neurol 2017;287:384–94.
[6] He Z, Jin Y. Intrinsic control of axon regeneration. Neuron 2016;90(3):437–51.
[7] Anderson MA, Burda JE, Ren Y, Ao Y, O'Shea TM, Kawaguchi R, et al. Astrocyte scar formation aids central nervous system axon regeneration. Nature 2016;532(7598):195–200.
[8] Mar FM, Bonni A, Sousa MM. Cell intrinsic control of axon regeneration. EMBO Rep 2014;15(3):254–63.
[9] Wei Y, Tsang CK, Zheng XFS. Mechanisms of regulation of RNA polymerase III-dependent transcription by TORC1. EMBO J 2009;28(15):2220–30.
[10] Michels AA, Robitaille AM, Buczynski-Ruchonnet D, Hodroj W, Reina JH, Hall MN, et al. mTORC1 directly phosphorylates and regulates human Maf1. Mol Cell Biol 2010;30(15):3749–57.
[11] Rideout EJ, Marshall L, Grewal SS. Drosophila RNA polymerase III repressor Maf1 controls body size and developmental timing by modulating tRNA(i)(Met) synthesis and systemic insulin signaling. Proc Natl Acad Sci USA 2012;109(4):1139–44.
[12] Boguta M. Maf1, a general negative regulator of RNA polymerase III in yeast. Biochimica et Biophysica Acta (BBA) - Gene Regul Mech 2013;1829(3–4):376–84.
[13] Johnson SS, Zhang C, Fromm J, Willis IM, Johnson DL. Mammalian Maf1 is a negative regulator of transcription by all three nuclear RNA polymerases. Mol Cell 2007;26(3):367–79.
[14] Upadhya R, Lee J, Willis IM. Maf1 is an essential mediator of diverse signals that repress RNA polymerase III transcription. Mol Cell 2002;10(6):1489–94.
[15] Boguta M, Czerska K, Żołądek T. Mutation in a new gene Maf1 affects tRNA suppressor efficiency in *Saccharomyces cerevisiae*. Gene 1997;185(2):291–6.
[16] Pluta K, Lefebvre O, Martin NC, Smagowicz WJ, Stanford DR, Ellis SR, et al. Maf1p, a negative effector of RNA polymerase III in *Saccharomyces cerevisiae*. Mol Cell Biol 2001;21(15):5031–40.
[17] Vannini A, Ringel R, Kusser AG, Berninghausen O, Kassavetis GA, Cramer P. Molecular basis of RNA polymerase III transcription repression by Maf1. Cell 2010;143(1):59–70.
[18] Willis IM. Maf1 phenotypes and cell physiology. Biochimica et Biophysica Acta (BBA) - Gene Regul Mech 2017.
[19] Khanna A, Johnson Deborah L, Curran SP. Physiological roles for mafr-1 in reproduction and lipid homeostasis. Cell Rep 2014;9(6):2180–91.
[20] Li Y, Tsang CK, Wang S, Li X-X, Yang Y, Fu L, et al. Maf1 suppresses AKT-mTOR signaling and liver cancer through activation of PTEN transcription. Hepatology 2016;63(6):1928–42.
[21] Palian BM, Rohira AD, Johnson SA, He L, Zheng N, Dubeau L, et al. Maf1 is a novel target of PTEN and PI3K signaling that negatively regulates oncogenesis and lipid metabolism. PLoS Genet 2014;10(12):e1004789.
[22] Burry RW. Protein synthesis requirement for the formation of synaptic elements. Brain Res 1985;344(1):109–19.
[23] Jung H, Yoon BC, Holt CE. Axonal mRNA localization and local protein synthesis in nervous system assembly, maintenance and repair. Nat Rev Neurosci 2012;13(5):308–24.
[24] Ryanne W-M, Jan Van M, Naweed IS. Synapse formation and plasticity: the roles of local protein synthesis. Neuroscientist 2005;11(3):228–37.
[25] Slomnicki LP, Pietrzak M, Vashishta A, Jones J, Lynch N, Elliot S, et al. Requirement of neuronal ribosome synthesis for growth and maintenance of the dendritic tree. J Biol Chem 2016;291(11):5721–39.
[26] Blackshaw S, Harpavat S, Trimarchi J, Cai L, Huang H, Kuo WP, et al. Genomic analysis of mouse retinal development. PLoS Biol 2004;2(9):e247.
[27] Smith K, Oliver P, Lumb M, Arancibia-Carcamo I, Revilla-Sanchez R, Brandon N, et al. Identification and characterisation of a Maf1/Macoco protein complex that interacts with GABAA receptors in neurons. Mol Cell Neurosci 2010;44(4):330–41.
[28] Joy MT, Ben Assayag E, Shabashov-Stone D, Liraz-Zaltsman S, Mazzitelli J, Arenas M, et al. CCR5 Is a therapeutic target for recovery after stroke and traumatic brain injury. Cell 2019;176(5).
[29] Overman JJ, Clarkson AN, Wanner IB, Overman WT, Eckstein I, Maguire JL, et al. A role for ephrin-A5 in axonal sprouting, recovery, and activity-dependent plasticity after stroke. 2012;109(33):E2230–E9.
[30] Lee G, Kim S, Homayouni R, D'Arcangelo G. Dab2ip regulates neuronal migration and neurite outgrowth in the developing neocortex. PLoS ONE 2012;7(10):e46592.
[31] Ventruti A, Kazdoba T, Niu S, D'Arcangelo G. Reelin deficiency causes specific defects in the molecular composition of the synapses in the adult brain. Neuroscience 2011;189:32–42.
[32] Niu S, Renfro A, Quattrocchi C, Sheldon M, D'Arcangelo G. Reelin promotes hippocampal dendrite development through the VLDLR/ApoER2-Dab1 pathway. Neuron 2004;41(1):71–84.
[33] Tsang C, Liu H, Zheng X. mTOR binds to the promoters of RNA polymerase I- and III-transcribed genes. Cell Cycle 2010;9(5):953–7.
[34] Kantidakis T, Ramsbottom BA, Birch JL, Dowding SN, White RJ. mTOR associates with TFIIIC, is found at tRNA and 5S rRNA genes, and targets their repressor Maf1. PNAS 2010;107(26):11823–8.
[35] Marshall L, Kenneth N, White R. Elevated tRNA(iMet) synthesis can drive cell proliferation and oncogenic transformation. Cell 2008;133(1):78–89.
[36] Nolan T, Hands RE, Bustin SA. Quantification of mRNA using real-time RT-PCR. Nat Protocols 2006;1(3):1559–82.
[37] Baskin YK, Dietrich WD, Green EJ. Two effective behavioral tasks for evaluating sensorimotor dysfunction following traumatic brain injury in mice. J Neurosci Methods 2003;129(1):87–93.
[38] Bouet V, Boulouard M, Toutain J, Divoux D, Bernaudin M, Schumann-Bard P, et al. The adhesive removal test: a sensitive method to assess sensorimotor deficits in mice. Nat Protoc 2009;4(10):1560–4.
[39] Clarkson AN, Huang BS, MacIsaac SE, Mody I, Carmichael ST. Reducing excessive GABA-mediated tonic inhibition promotes functional recovery after stroke. Nature 2010;468:305.
[40] Longair MH, Baker DA, Armstrong JD. Simple Neurite Tracer: open source software for reconstruction, visualization and analysis of neuronal processes. Bioinformatics 2011;27(17):2453–4.
[41] Kaya-Okur HS, Wu SJ, Codomo CA, Pledger ES, Bryson TD, Henikoff JG, et al. CUT&Tag for efficient epigenomic profiling of small samples and single cells. Nat Commun 2019;10(1):1930.
[42] Xie X, Li M, Zhou M, Chow SF, Tsang CK. Pharmacological preconditioning by TERT inhibitor BIBR1532 confers neuronal ischemic tolerance through TERT-mediated transcriptional reprogramming. J Neurochem 2021;159(4):690–709.
[43] Langmead B, Salzberg SL. Fast gapped-read alignment with Bowtie 2. Nat Methods 2012;9(4):357–9.
[44] Zhang Y, Liu T, Meyer CA, Eeckhoute J, Johnson DS, Bernstein BE, et al. Model-based analysis of ChIP-Seq (MACS). Genome Biol 2008;9(9):R137.
[45] Thorvaldsdóttir H, Robinson JT, Mesirov JP. Integrative Genomics Viewer (IGV): high-performance genomics data visualization and exploration. Brief Bioinform 2013;14(2):178–92.
[46] Huang da W, Sherman BT, Lempicki RA. Systematic and integrative analysis of large gene lists using DAVID bioinformatics resources. Nat Protoc 2009;4(1):44–57.
[47] Huang da W, Sherman BT, Lempicki RA. Bioinformatics enrichment tools: paths toward the comprehensive functional analysis of large gene lists. Nucleic Acids Res 2009;37(1):1–13.
[48] Geiduschek E, Kassavetis G. Transcription: adjusting to adversity by regulating RNA polymerase. Curr Biol 2006;16(19):R849–51.
[49] Willis I, Moir R. Integration of nutritional and stress signaling pathways by Maf1. Trends Biochem Sci 2007;32(2):51–3.

[50] Goodfellow S, Graham E, Kantidakis T, Marshall L, Coppins B, Oficjalska-Pham D, et al. Regulation of RNA polymerase III transcription by Maf1 in mammalian cells. J Mol Biol 2008;378(3):481–91.
[51] Shor B, Wu J, Shakey Q, Toral-Barza L, Shi C, Follettie M, et al. Requirement of the mTOR kinase for the regulation of Maf1 phosphorylation and control of RNA polymerase III-dependent transcription in cancer cells. J Biol Chem 2010;285(20):15380–92.
[52] Jossin Y, Goffinet AM. Reelin signals through phosphatidylinositol 3-kinase and Akt to control cortical development and through mTor To regulate dendritic growth. Mol Cell Biol 2007;27(20):7113–24.
[53] Niu S, Yabut O, D'Arcangelo G. The Reelin signaling pathway promotes dendritic spine development in hippocampal neurons. J Neurosci 2008;28 (41):10339–48.
[54] Chan KY, Jang MJ, Yoo BB, Greenbaum A, Ravi N, Wu WL, et al. Engineered AAVs for efficient noninvasive gene delivery to the central and peripheral nervous systems. Nat Neurosci 2017;20(8):1172–9.
[55] Deverman BE, Pravdo PL, Simpson BP, Kumar SR, Chan KY, Banerjee A, et al. Cre-dependent selection yields AAV variants for widespread gene transfer to the adult brain. Nat Biotechnol 2016;34(2):204–9.
[56] Hetman M, Pietrzak M. Emerging roles of the neuronal nucleolus. Trends Neurosci 2012;35(5):305–14.
[57] Moon LDF. Chromatolysis: do injured axons regenerate poorly when ribonucleases attack rough endoplasmic reticulum, ribosomes and RNA? Dev Neurobiol 2018;78(10):1011–24.
[58] Mahar M, Cavalli V. Intrinsic mechanisms of neuronal axon regeneration. Nat Rev Neurosci 2018;19(6):323–37.
[59] Johannessen M, Delghandi MP, Moens U. What turns CREB on? Cell Signal 2004;16(11):1211–27.
[60] Goodfellow S, White R. Regulation of RNA polymerase III transcription during mammalian cell growth. Cell Cycle 2007;6(19):2323–6.
[61] Zhang S, Li X, Wang HY, Steven Zheng XF. Beyond regulation of pol III: Role of Maf1 in growth, metabolism, aging and cancer. Biochim Biophys Acta Gene Regul Mech 2018;1861(4):338–43.
[62] Silva AJ, Kogan JH, Frankland a PW, Kida S. Creb and memory. Annu Rev Neurosci. 1998;21(1):127–48.
[63] Lonze BE, Riccio A, Cohen S, Ginty DD. Apoptosis, axonal growth defects, and degeneration of peripheral neurons in mice lacking CREB. Neuron 2002;34 (3):371–85.
[64] Redmond L, Kashani AH, Ghosh A. Calcium regulation of dendritic growth via CaM kinase IV and CREB-mediated transcription. Neuron 2002;34(6):999–1010.
[65] Gao Y, Deng K, Hou J, Bryson JB, Barco A, Nikulina E, et al. Activated CREB is sufficient to overcome inhibitors in myelin and promote spinal axon regeneration in vivo. Neuron 2004;44(4):609–21.
[66] Caracciolo L, Marosi M, Mazzitelli J, Latifi S, Sano Y, Galvan L, et al. CREB controls cortical circuit plasticity and functional recovery after stroke. Nat Commun 2018;9(1):2250.
[67] Clarkson AN, Parker K, Nilsson M, Walker FR, Gowing EK. Combined ampakine and BDNF treatments enhance poststroke functional recovery in aged mice via AKT-CREB signaling. J Cereb Blood Flow Metab 2015;35(8):1272–9.
[68] Chen K, Zhu L, Guo L, Pan YB, Feng DF. Maf1 regulates dendritic morphogenesis and influences learning and memory. Cell Death Dis 2020;11(7):606.
[69] Chen D, Sun YY, Zhou LY, Yang S, Hong FY, Liu XD, et al. Maf1 regulates axonal regeneration of retinal ganglion cells after injury. Exp Neurol 2022;348:113948.
[70] Abe N, Borson SH, Gambello MJ, Wang F, Cavalli V. Mammalian target of rapamycin (mTOR) activation increases axonal growth capacity of injured peripheral nerves. J Biol Chem 2010;285(36):28034–43.
[71] Huang H, Miao L, Yang L, Liang F, Wang Q, Zhuang P, et al. AKT-dependent and -independent pathways mediate PTEN deletion-induced CNS axon regeneration. Cell Death Dis 2019;10(3):203.
[72] Park KK, Liu K, Hu Y, Smith PD, Wang C, Cai B, et al. Promoting axon regeneration in the adult CNS by modulation of the PTEN/mTOR Pathway. Science (New York, NY) 2008;322(5903):963–6.
[73] Endersby R, Baker SJ. PTEN signaling in brain: neuropathology and tumorigenesis. Oncogene 2008;27(41):5416–30.
[74] Song MS, Salmena L, Pandolfi pp. The functions and regulation of the PTEN tumour suppressor. Nat Rev Mol Cell Biol 2012;13(5):283–96.
[75] Bonhoure N, Byrnes A, Moir RD, Hodroj W, Preitner F, Praz V, et al. Loss of the RNA polymerase III repressor Maf1 confers obesity resistance. Genes Dev 2015;29(9):934–47.
[76] Chen R, Wen D, Fu W, Xing L, Ma L, Liu Y, et al. Treatment effect of DNA framework nucleic acids on diffuse microvascular endothelial cell injury after subarachnoid hemorrhage. Cell Prolif 2022;55(4):e13206.
[77] Fu W, Ma L, Ju Y, Xu J, Li H, Shi S, et al. Therapeutic siCCR2 loaded by tetrahedral framework DNA nanorobotics in therapy for intracranial hemorrhage (Adv. Funct. Mater. 33/2021). Adv Funct Mater 2021;31 (33):2170239.
[78] Li J, Yao Y, Wang Y, Xu J, Zhao D, Liu M, et al. Modulation of the crosstalk between Schwann cells and macrophages for nerve regeneration: a therapeutic strategy based on a multifunctional tetrahedral framework nucleic acids system. Adv Mater 2022.
[79] Zhou M, Zhang T, Zhang B, Zhang X, Gao S, Zhang T, et al. A DNA nanostructure-based neuroprotectant against neuronal apoptosis via inhibiting toll-like receptor 2 signaling pathway in acute ischemic stroke. ACS Nano 2022;16 (1):1456–70.
[80] Li MX, Weng JW, Ho ES, Chow SF, Tsang CK. Brain delivering RNA-based therapeutic strategies by targeting mTOR pathway for axon regeneration after central nervous system injury. Neural Regener Res 2022;17 (10):2157–65.
[81] Labat-gest V, Tomasi S. Photothrombotic ischemia: a minimally invasive and reproducible photochemical cortical lesion model for mouse stroke studies. J Vis Exp 2013;76.